How split-feed osmotically assisted reverse osmosis (SF-OARO) can outperform conventional reverse osmosis (CRO) processes under constant and varying electricity tariffs

Zijing Mo[a,b,c,1], Christian D. Peters[d,1], Cheng Long[e], Nicholas P. Hankins[d], Qianhong She[a,b,*]

[a] Singapore Membrane Technology Centre, Nanyang Environment and Water Research Institute, Nanyang Technological University, 1 Cleantech Loop, Clean Tech One 06-08, Singapore 637141

[b] School of Civil and Environmental Engineering, Nanyang Technological University, 50 Nanyang Avenue, Singapore 639798

[c] Interdisciplinary Graduate Programme, Nanyang Technological University, 50 Nanyang Avenue, Singapore 639798

[d] Department of Engineering Science, The University of Oxford, Parks Road, OX3 1PJ Oxford, UK

[e] School of Computer Science and Engineering, Nanyang Technological University, 50 Nanyang Avenue, Singapore 639798

[1] These authors contributed equally to this work

* Corresponding author, E-mail: qhshe@ntu.edu.sg

Nomenclature

Symbols	Parameter	Unit
A	Membrane water permeability	LMH/bar
A_{RO}	RO membrane water permeability	LMH/bar
A_{OA}	OARO membrane water permeability	(LMH=L.m^{-2}h^{-1})
$Area_{mem}$	Membrane surface area	m^2
B	Membrane salt permeability	LMH
B_{RO}	RO membrane salt permeability	LMH
B_{OA}	OARO membrane salt permeability	LMH
C_P	Permeate concentration	mol.L^{-1}
C_{PT}	Permeate concentration target	mol.L^{-1}
C_n $(n \in \mathbb{N}^*_{\leq 8})$	Concentration of stream n in the SF-OARO system	mol.L^{-1}
C_{SW}	Seawater salinity	mol.L^{-1}
$CapEx$	Capital cost of the desalination system	\$/year
$CapEx_{Mem}$	Capital cost of membrane	\$/m^3
$CapEx_{HPP}$	Capital cost of high-pressure pump	\$/(bar. m^3/hr)
$CapEx_{BP}$	Capital cost of booster pump	\$/(bar. m^3/hr)
$CapEx_{PX}$	Capital cost of pressure exchanger	\$/(m^3/hr)
$CapEx_{PV}$	Capital cost of pressure vessel	\$/vessel
$CapEx_{In}$	CapEx for intake and pre-treatment	\$/(m^3/hr)
D	Diffusivity coefficient	m^2/hr
Ep	Electricity price	\$/kWh
Ep_{avg}	Average electricity price	\$/kWh
f_c	Capitalisation factor	%/year
f_I	Practical investment factor	-
i	The sequence of segment	
K_i	Overall mass transfer coefficient at ith	m/hr
$k_{D,i}$	Permeate side mass transfer coefficient at i^{th} segment	m/hr
$k_{F,i}$	Feed side mass transfer coefficient at i^{th} segment	m/hr
k_m	Membrane intrinsic mass transfer coefficient	m/hr
$J_{s,i}$	Solute flux at i^{th} segment	mol.m^{-2}h^{-1}
$J_{w,i}$	Water flux at i^{th} segment	LMH

j	Sequence of shooting	
N_{OA}	Number of module per RO pressure vessel	-
N_{RO}	Number of module per OARO pressure vessel	-
$n_{PV,RO}$	Number of RO pressure vessels	-
$n_{PV,OA}$	Number of OARO pressure vessels	-
$OpEx$	Annual operational cost of the system	\$/year
O_{Re}	Annual membrane replacement cost	\$/year
O_{ML}	Annual membrane maintenance cost	\$/year
O_{Elec}	Annual electricity cost	\$/year
O_B	Brine disposal cost	\$/m^3
P_{OA}	Applied pressure of the OARO module	bar
P_a	Applied pressure to the RO module for SF-OARO and CRO system	bar
$P_{OA,B}$	Brine outflow pressure of the OARO module	bar
$P_{RO,B}$	Brine outflow pressure of the RO module	bar
P_M	Maximum operating pressure of membrane	bar
$P_{F,i}$	Pressure of feed side solution at i^{th} segment	m^3/hr
Q_n $(n \in \mathbb{N}^*_{\leq 8})$	Flowrate of stream n in the SF-OARO system	m^3/hr
Q_{OA}	Feed flowrate per OARO pressure vessel	m^3/hr
Q_{RO}	Feed flowrate per RO pressure vessel	m^3/hr
Q_F	Feed flowrate of the osmosis system	m^3/hr
Q_B	Brine flowrate of the osmosis system	
Q_P	Permeate flowrate of the osmosis system	m^3/hr
R_g	Ideal gas constant	L.bar/(K/mol)
RR_{OA}	Water recovery ratio of the OARO module	-
RR_S	Water recovery ratio of the desalination system	-
Re	Reynolds number	-
r_i	Interest rate	-
S	Structural parameter of membrane	mm
S_{OA}	Structural parameter of membrane in OARO module	mm
Sc	Schmidt number	-
$SEC_{CRO,ideal}$	Ideal specific energy consumption of CRO	kWh/m^3
$SEC_{d1,ideal}$	Ideal specific energy consumption of SF-OARO design 1	kWh/m^3

$SEC_{d2,ideal}$	Ideal specific energy consumption of SF-OARO design 2	kWh/m^3
$SEC_{d1,deff}$	Specific energy consumption of SF-OARO design 1 with consideration of pump and PX deficiencies	kWh/m^3
$SEC_{d2,deff}$	Specific energy consumption of SF-OARO design 2 with consideration of pump and PX deficiencies	kWh/m^3
SEC_{prac}	Practical specific energy consumption of SF-OARO system	kWh/m^3
Sh	Sherwood number	-
SR	Split ratio of RO brine entering OARO module	-
t_1	Length of variable operation mode time period 1	hr
t_2	Length of variable operation mode time period 2	hr
T	Temperature of environment	K
W_1	Production scale factor	-
W_2	Permeate quality scale factor for period 1	-
W_3	Permeate quality scale factor for period 2	-
$\vec{a}_{1\times 5}$	Input vector for the SFR-mode SF-OARO system	-
$\vec{a}_{1\times 9}$	Input vector for the TOU-mode SF-OARO system	-
β	van't Hoff factor	-
η_{PX}	Efficiency of pressure exchanger	-
η_{pump}	Pump efficiency	-
$\pi_{D,i}$	Permeate osmotic pressure at segment i	bar
$\pi_{F,i}$	Feed osmotic pressure at segment i	bar
π_n $(n \in \mathbb{N}^*_{\le 8})$	Osmotic pressure of stream n in the SF-OARO system	bar

Abbreviations

Abbreviation	Meaning
AWP	Annual water production
BP	Booster pump
BVM	Brine volume minimization
C-OARO	Cascading osmotically assisted reverse osmosis
CP	Concentration polarization
CRO	Conventional single-stage reverse osmosis
ECP	External concentration polarization
ERD	Energy recovery device
GD	Gradient decent
HP	High-pressure pump
HPRO	High pressure reverse osmosis
HSBRO	Hybrid system brine RO
ICP	Internal concentration polarization
LSRRO	Low salt rejection reverse osmosis
LM	Levenberg-Marquardt algorithm
MP-OARO	Multi-pass osmotically assisted reverse osmosis
MSRO	Multi-stage reverse osmosis
OPF	Optimal function
PL	Plant life
PSA	Porcellio scaber algorithm
PX	Pressure exchanger
PV	Pressure vessel
RTP	Real time pricing
SEC	Specific energy consumed per m^3 water production
SF-OARO	Split-feed osmotically assisted reverse osmosis
SFR	Standard flat rate
SQP	Sequential quadratic programming algorithm
TAC	Total annual cost for water production
TFC	Thin film composite
TMP	Transmembrane pressure
TOU	Time of use
UWC	Unit water cost

Abstract

Improving the recovery of desalination processes can have economic benefits, as feed and brine volumes are minimised. Furthermore, brine volume minimisation (BVM) simplifies brine treatment prior to disposal and hence, alleviates potential environmental concerns. However, BVM is not widely applied, as it is generally more energy intensive and costly. This may change in the future, as new high-recovery membrane processes, such as split-feed osmotically assisted reverse osmosis (SF-OARO), can potentially lower the required operating pressure and the energy consumption associated with brine dewatering via osmotic counterbalance. In addition, the added flexibility of OARO integrated systems may further reduce the unit water cost (UWC) in regions with varying-electricity tariffs. To verify these hypothesised advantages of OARO, this study explores the economic and technical viability of SF-OARO. Under constant electricity tariffs, the results indicate that the optimized SF-OARO process can achieve a higher process recovery (65% versus 50%) while operating at a 4.1% lower UWC than conventional RO (CRO), when assuming an intermediate brine disposal cost of 0.3 $/m^3$. This cost advantage of SF-OARO further expands under operation with varying-electricity tariffs. In summary, the presented results indicate that the SF-OARO process is the preferred and cheaper choice once the brine disposal cost exceeds 0.21 $ per cubic meter of brine.

Keywords:

Osmotically assisted reverse osmosis (OARO); Split-feed counterflow reverse osmosis (CFRO); Dynamic desalination operation; Varying electricity tariffs; Brine volume minimization (BVM)

1. Introduction

Desalination faces several hurdles to becoming truly sustainable and affordable. The grand challenge for the desalination industry is to produce freshwater with a lower environmental impact and at a lower cost. Environmental concerns of desalination include (1) its high energy consumption, which is responsible for its large carbon footprint, and (2) the discharge of untreated brine that is often severely polluted by contaminants, such as anti-fouling and anti-scaling additives, anti-foaming additives, oxygen scavengers and corrosion products [1, 2].

The high energy consumption and the treatment and discharge of brine also make desalination costly. Among the currently available desalination technologies, reverse osmosis (RO) is the most widely applied desalination technology and requires anywhere from 2 kWh to 5.2 kWh per cubic meter of freshwater [3, 4]. In terms of cost, the RO unit water cost (UWC) can be as low as 0.28 $\$/m^3$ (excluding brine disposal cost) for large-scale, high-efficiency plants [5]. While electricity costs are the main contributor to the overall UWC, brine disposal costs can constitute anywhere between 5% and 33% of the total cost of desalination [6]. A reduction in brine volume can lower the incurred costs associated with its disposal and treatment, and this reduction may be required to meet local regulations [7] and to reduce its environmental impact [8]. Therefore, to address the environmental and economic concerns of desalination, the development of energy-efficient brine volume minimisation (BVM) technologies is vital. For low recovery desalination, the conventional RO (CRO) process with a single-stage design is currently the favoured method in the industry, due to its low cost and robustness [4]. However, the maximum recovery of the CRO process is limited by the membrane's burst pressure. In addition, CRO becomes less energy efficient when the recovery is increased, due to proportionately greater irreversible losses incurred by constant pressure operation [3, 9]. These irreversible losses can, for example, be minimised by multi-stage design (MSRO) [10].

MSRO separates the dewatering process into multiple stages with different exiting brine salinities, which reduces the minimum hydraulic pressure requirement in the preceding steps. Batch RO systems can also be categorised as multi-stage processes and are able to save energy by continuously increasing the operating pressure with the process recovery to minimise the irreversible losses [11, 12]. Examples of batch design include batch RO, closed-circuit RO (CCRO) [3] and hybrid system brine RO (HSBRO) [13]. However, despite their different designs, the minimum hydraulic pressure applied at the brine exiting stage cannot be lower than the osmotic pressure of the brine, the latter increasing with recovery. Therefore, the recovery of MSRO seawater desalination systems remains limited to 50% due to the pressure threshold of most commercial membranes [14]. High-pressure RO (HPRO) membranes and modules have been developed with advanced mechanical strengths to withstand hydraulic pressures of over 100 bar [14]. There are, however, several issues associated with high-pressure operation, such as lower-than-expected water fluxes due to membrane compaction [15] and the introduction of additional challenges for piping, pumping, and pressure vessel design [16], all of which lead to surging capital costs for plant design and operation . Moreover, the limited choice of HPRO elements (such as Dupont XUS180808) and their high cost [17] further dampen the economic feasibility of multi-stage or batch designs for BVM at high recoveries.

It should be noted that there are, other purely pressure-driven membrane process configurations, such as low-salt-rejection reverse osmosis (LSRRO), that can be utilised for BVM [18]. Wang et al. [18] showed that LSRRO can dewater hypersaline brines of up to 4.0 M NaCl at moderate pressures of 70 bar. It is evident that the membrane's salt rejection in LSRRO becomes a pivotal factor that directly affects the specific energy consumption (SEC) and the product water quality. This membrane property (i.e., salt rejection) is mainly dependent on the chosen membrane and cannot be flexibly mediated by operational changes. This makes it more complicated to tweak the process to operate under optimum conditions.

To circumvent the limitations of purely pressure-driven membrane processes, this study focuses on osmotically assisted desalination technologies [19]. The use of a draw solution (i.e., salt water) at the permeate side of reverse osmosis, which gives rise to osmotically assisted reverse osmosis (OARO) processes, has the distinct benefit of enabling these processes to operate at lower hydraulic pressures while still being able to dewater highly saline brines. Previous studies have highlighted the potential of OARO to achieve high system recoveries at relatively low transmembrane pressures and low energy consumptions [19-21]. For example, Chen et al. [21] showed that a two-stage OARO system could achieve a 70% system recovery at a SEC of 2.7 kWh/m^3 while the maximum operating pressure did not exceed 70 bar.

Another advantage of OARO is its operational flexibility. In comparison to LSRRO, the recovery and SEC of the system are dependent not only on the membrane's selectivity, but also on an additional hydrodynamically controllable parameter, namely the split or recovery ratio (SR). This ratio describes the difference in volume between the OARO feed and draw streams and could potentially be used to achieve the desired process recovery at the lowest possible SEC [19, 20], Furthermore, the combination of several membrane processes into a single system (e.g., RO+OARO) offers additional degrees of freedom when compared to CRO. This added flexibility of RO+OARO combined processes allows for operation across a wider range of recoveries, and can therefore be utilised to better operate under time-varying conditions. Split-feed OARO is a form of RO+OARO process in which the concentrate from the RO module is split into two streams entering the feed and draw side of the OARO module. The diluted stream from the OARO module is recycled and mixed with the fresh feed. The mixed solution is fed to the RO module to produce fresh water. A study by Peters et al. [20] shows that SF-OARO achieves a lower SEC, is operable at technically feasible pressures and is more compact than other OARO configurations, such as Cascading OARO (C-OARO) and Multi-pass OARO (MP-OARO).

While SF-OARO is a promising BVM technology, the question still remains as to how it can outperform CRO in terms of energy efficiency and cost. To answer this question, a direct and numerical comparison between the CRO and SF-OARO processes is performed in this study. In the SF-OARO, the concentrate from the RO stage is split into two streams to enter the feed and permeate side of the OARO module. In this study, situations are investigated in which the operational flexibility and the high-recovery of OARO can be fully utilised to minimise the UWC. Firstly, the CRO and SF-OARO processes are compared at constant electricity pricing for varying brine discharge costs. It is expected that, due to the high recovery of OARO, the SF-OARO process will outperform the CRO process in situations where the brine discharge costs are higher (e.g., inland desalination [1, 22]). Secondly, the SF-OARO and CRO processes are compared under time-varying electricity tariffs. This is especially interesting due to the growing supply of electricity from sustainable but unsteady power sources (i.e., wind and solar). With the incorporation of sustainable power sources, and due to the varying electricity demand throughout the day, the supply and cost of electricity vary more severely throughout the day [23]. Adopting the time-of-use (TOU) pricing systems would accommodate for the varying time-value of electricity. The cost analysis is based on a constant intake capacity of 20,000 m^3/hr and a maximum permeate concentration of 0.01 M (0.6 g/L M NaCl) [24]. Furthermore, three different TOU scenarios are considered during which the UWC of the SF-OARO system is further reduced by adapting the variate operating mode.

As introduced by Bartholomew et al [25], the optimisation of OARO integrated systems is generally based on a one-factor-at-a-time (OFAT) analysis, neglecting higher-degree interactions between operating parameters. Therefore, the flexibility of the OARO system cannot be fully utilised. Unlike OFAT analysis, the OARO operating parameters are simultaneously optimised in this study, revealing its full potential to achieve the minimal UWC. This is done by converting the optimisation problem into a non-linear multi-variate problem using mathematical modelling. To circumvent convergence to local minima, we introduced the bio-inspired semi-discrete algorithm, Porcellio Scaber Algorithm (PSA), in our optimisation to obtain rough global minima for the complex non-linear constrained problem [26]. These rough minima from the PSA algorithm were then used as initial guesses for the conventional batch gradient descent (BGD) algorithm to obtain the accurate optimal condition for the SF-OARO process.

2. Methodology

2.1 Ideal case study

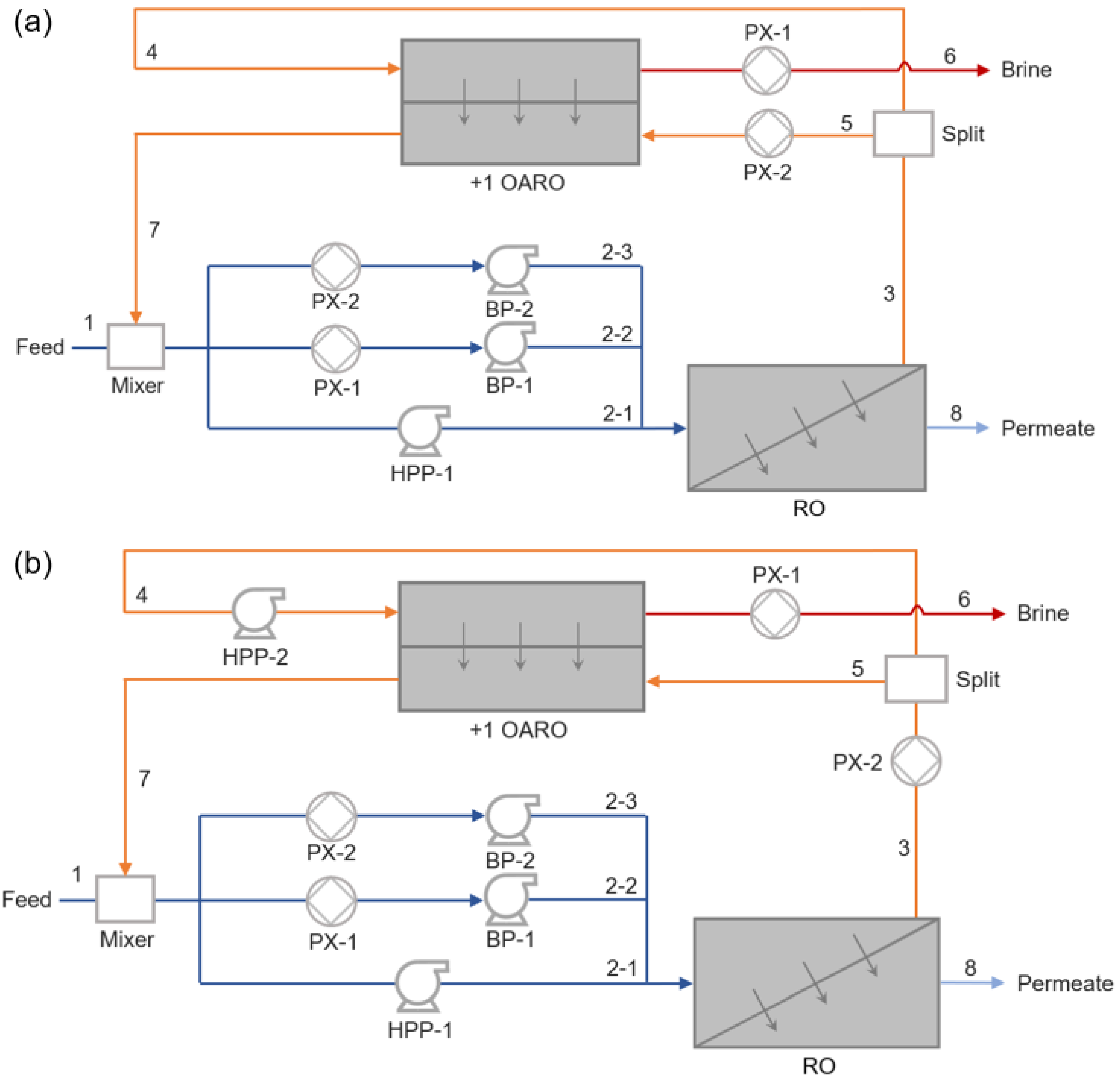

Figure 1. SF-OARO a) Design 1 b) Design 2 for ideal case and practical system calculation. HPP: high pressure pump BP: booster pump. PX: pressure exchanger.

Ideal SECs for CRO and SF-OARO configuration are first calculated and compared in this subsection, respectively. For the ideal case friction pressure losses, concentration polarization (CP) salt permeation, pressure exchanger (PX) and pump inefficiencies and over-pressurization are neglected. Furthermore, unlimited membrane areas are assumed. Assuming that the hydraulic pressure of the brine stream can be fully recovered, the ideal SEC of CRO can be expressed as,

$$SEC_{CRO,ideal} = \frac{Q_F \times P_a - Q_B \times P_a}{Q_P} = P_a \tag{1}$$

where Q_F , Q_B and Q_P are the feed, brine and permeate flowrate of the desalination system, respectively. P_a is the applied pressure of the RO system.

Two different SF-OARO layouts are discussed in the ideal case study, both of which are depicted in

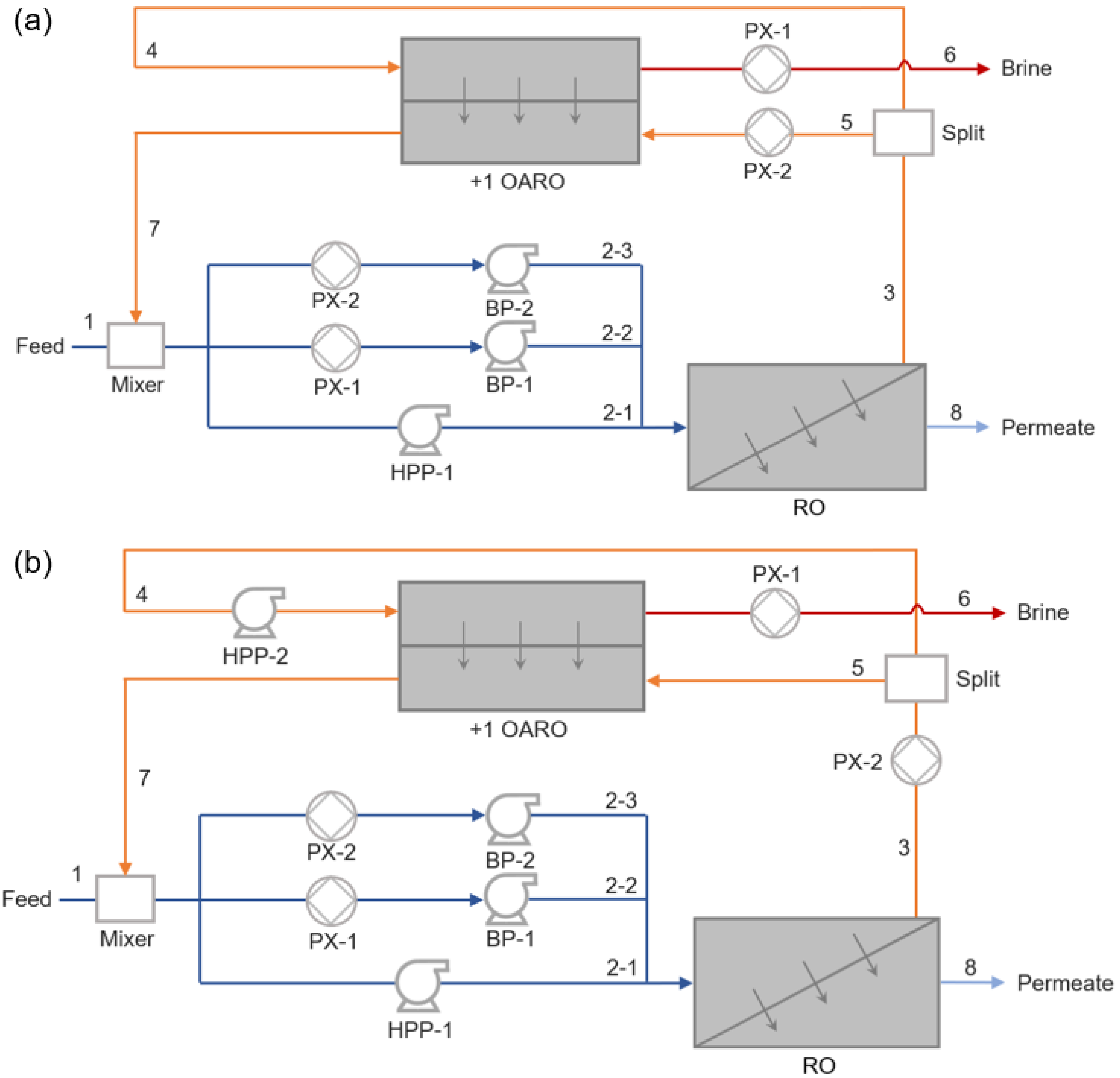

Figure 1. Both designs utilise a single split-feed counterflow OARO stage to further concentrate the brine solution exiting the RO stage. The difference between the two designs is that in Design 1 the RO and OARO stage are operated at the same hydraulic pressure, whereas in Design 2 the OARO stage can be operated at a pressure different to that of the RO stage. In design 2, the OARO operating pressure can be adjusted to a lower level than the RO operating pressure, which might be more adaptive when the OARO membrane burst pressure is below that of the RO membrane However, an additional set of high-pressure pump (HPP), is required, which increases the overall capital costs of Design 2 since HPP is the major contributor to the capital. Despite the different configurations, the system water recovery, RR_S, of both designs is defined as:

$$RR_S = \frac{Q_8}{Q_1} \tag{2}$$

Two additional variables are introduced to describe the OARO operation. One is the water recovery ratio of the OARO module, RR_{OA}, as expressed below

$$RR_{OA} = \frac{Q_4 - Q_6}{Q_4} \tag{3}$$

The other one is the split ratio of OARO draw flow rate (Q_5) to OARO feed flow rate (Q_4), SR, which is defined as:

$$SR = \frac{Q_5}{Q_4} \tag{4}$$

For each specific system recovery RR_S, stream properties of the SF-OARO processes can be expressed by functions of RR_{OA} and SR as listed in Table 1. The inlet seawater salinity C_{SW} is kept constant at 0.6M.

Table 1. Flowrate and salt concentration in different streams of the SF-OARO integrated system.

Stream No.	Q (m^3/h)	C (mol/L)
1	Q_F	C_{SW}
2	$Q_F\left(\frac{1-RR_S}{1-RR_{OA}} \times (SR+1) + RR_S\right)$	$\frac{C_{SW} \times (SR+1)}{\frac{1-RR_S}{1-RR_{OA}} \times (SR+1) + RR_S}$
3	$Q_F \times \frac{1-RR_S}{1-RR_{OA}} \times (SR+1)$	$\frac{C_{SW} \times (1-RR_{OA})}{1-RR_S}$
4	$Q_F \times \frac{1-RR_S}{1-RR_{OA}}$	$\frac{C_{SW} \times (1-RR_{OA})}{1-RR_S}$
5	$Q_F \times \frac{1-RR_S}{1-RR_{OA}} \times SR$	$\frac{C_{SW} \times (1-RR_{OA})}{1-RR_S}$
6	$Q_F(1-RR_S)$	$\frac{C_{SW}}{(1-RR_S)}$
7	$Q_F \times \left(\frac{1-RR_S}{1-RR_{OA}} \times (SR+1) - (1-RR_S)\right)$	$\frac{C_{SW} \times SR}{\frac{1-RR_S}{1-RR_{OA}} \times (SR+1) - (1-RR_S)}$
8	$Q_F RR_S$	*0*

The SEC of each design are developed based on mass balances, which are further detailed in Appendix

A. For Design 1, the OARO and RO membrane stages are operated at the same applied pressure, $P_{OA} = P_a = \beta R_g T C_3$, where β is the van't Hoff factor, hence,

$$SEC_{d1,ideal} = \frac{\beta R_g T C_{sw}\left(\frac{1-RR_S}{1-RR_{OA}} + 2RR_S - 1\right)(1-RR_{OA})}{RR_S(1-RR_S)} \tag{5}$$

For Design 2, the OARO and RO membrane stages are operated at different pressures ($P_{OA} \neq P_{RO}$). Utilizing pressure exchangers, stream 3 and 6 are depressurised to ambient pressure while HPP-2 is used to repressurise stream 4 to the target OARO operating pressure P_{OA}, therefore,

$$SEC_{d2,ideal} = \frac{\beta R_g T C_{SW}\left(\frac{{RR_{OA}}^2}{1-RR_{OA}} + \frac{1-RR_{OA}}{1-RR_S}RR_S\right)}{RR_S} \tag{6}$$

The optimal applied pressure P_{OA} equals to the maximum transmembrane osmotic pressure difference within the OARO module,

$$P_{OA} = \pi_6 - \pi_5 \tag{7}$$

For both designs, the optimal ideal SEC (i.e., SEC_{ideal}) can be obtained by minimising the 2-variable function $SEC_{ideal} = f(RR_{OA}, SR)$. This was done using the MATLAB fmincon function. After the ideal SEC was obtained, the SEC was determined when considering the pump efficiency (η_{pump} = 80%) and the pressure exchanger efficiency (η_{PX} = 98%),

$$SEC_{d1,deff} = \frac{\beta R_g T C_{SW}(1-RR_{OA}) \times \left(\left(\frac{(1-RR_S)(SR+1)}{1-RR_{OA}} + RR_S\right) - \eta_{PX} \times \left(\frac{(1-RR_S)\times SR}{1-RR_{OA}} + (1-RR_S)\right)\right)}{(1-RR_S)RR_S \times \eta_{pump}} \tag{8}$$

$$SEC_{d2,deff} = \beta R_g T C_{SW} \frac{\frac{(1-RR_{OA})}{1-RR_S} \times \left(\frac{1-RR_S}{1-RR_{OA}} \times (SR+1) + RR_S\right) + \frac{RR_{OA}}{1-RR_{OA}} - \eta_{PX}\left((SR+1) + RR_{OA}\right)}{RR_S \times \eta_{pump}} \tag{9}$$

2.2 Unit water cost (UWC) optimisation for the constant and variable electricity tariff scenarios

With the ideal, minimum energy consumption of the SF-OARO process calculated, a more practical model, which includes both ICP effects and finite membrane areas, was developed for the SF-OARO and CRO configuration. The governing equations used to model the membrane processes are given in Section 2.1. As mentioned previously, the UWC of both processes are compared over a wide range of recoveries (Y_S = 45 - 75%) for different electricity tariff scenarios. The UWC factors and the different electricity tariff scenarios are discussed in Sections 2.2.2 and Section 2.2.3, respectively.

As the plant's intake capacity Q_F is set as constant (20 000 m^3/hr), the total pre-treatment costs at different recovery ratios are set the same between the different processes by assuming that the same pre-treatment process is used and the pre-treatment can ensure the sufficient removal of foulants and inhibition of scaling[21, 27]. *Table 2* lists the selected operating and membrane parameters for the CRO and SF-OARO processes. A SW30-8040 module from Filmtec was chosen as a suitable RO module, owing to its commercial popularity, and an Aquaporin (AQP) based TFC membrane from Aquaporin A/S was chosen for the OARO process. In our previous study [28], this AQP membrane was fully characterised and was found suitable for OARO operation at pressures of up to 60 bar. Lastly, the salt concentration of the permeate is limited in the simulation to less than $C_{PT} = 0.01$ M to adhere to the WHO's drinking water standards [24].

Table 2. Characteristics of membranes, modules, PX and pumps used in calculation.

		Value	Unit	Ref.
A_{RO}	RO membrane water permeability	1.13	LMH/bar	[29]
A_{OA}	OARO membrane water permeability	2.49	LMH/bar	[20]
$Area_{mem}$	Membrane area per RO and OARO module	37.2	m^2	[29]
B_{RO}	RO membrane salt permeability	0.08	LMH	[29]
B_{OA}	OARO membrane salt permeability	0.39	LMH	[20]
D	Diffusion coefficient of sodium chloride	1.33×10^{-9}	m^2/s	[20]
N_{RO}	Number of elements per RO pressure vessel	7	-	[29]

N_{OA}	Number of elements per OARO pressure vessel	To be optimised	-	-
P_M [a]	Maximum operating pressure of RO and OARO membranes	69	bar	[30]
S_{OA}	Structural parameter of OARO membrane	Multiple values	mm	[20, 31, 32]
η_{PX}	Efficiency of PX	98%	-	[33]
η_{pump}	Efficiency of HPP and BP	80%	-	[12]

a. The maximum operating pressure P_M of the AQP membrane is assumed to be the same as that of the SW30 membrane (69 bar) [34]. An extra cost analysis was conducted in Appendix D using P_M=82 bar which is the recommended P_M for the new version of the SW30 module [30]. In either case, once the operating pressure exceeds P_M, a different HPRO membrane (Dupont XUS180808) is modelled for both the RO and OARO membrane stages.

2.2.1. OARO governing equations

The ideal case energy analysis laid out in Section 2.1 does not consider non-idealities, such as friction losses and concentration polarization (CP) effects [35]. In the practical OARO simulation, these non-idealities are included and the finite difference method (FDM) is used to obtain the water and solute flux across the length of the RO and OARO membrane modules. Using the FDM, the limited membrane area is divided into multiple segments. For the i^{th} segment of a RO or OARO module, the water flux across the membrane is $J_{w,\mathrm{i}}$ and can be described by the osmotic resistance filtration model given by Eqs. (10)-(11) [20, 36]. The active-layer-facing-feed side (AL-FS) membrane orientation is assumed for all membrane modules [36]. The water flux is given by:

$$J_{w,i} = A\left(P_{F,i} - (\pi_{F,i} - \pi_{D,i}) - \left(exp\left(\frac{J_{w,i}}{k_{F,i}}\right) - 1\right)\left(\pi_{F,i} - \frac{J_{s,i}}{J_{w,i}}\beta R_g T\right) + \left(1 - exp\left(-\frac{J_{w.i}}{K_i}\right)\right)\left(\pi_{D,i} + \frac{J_{s,i}}{J_{w,i}}\beta R_g T\right)\right) \tag{10}$$

and the solute flux across the membrane $J_{s,\mathrm{i}}$ can be described by:

$$J_{s,i} = \frac{B}{A\beta R_g T}\left(\frac{A \times P_{F,i}}{J_{w,i}} - 1\right)J_{w,i} \tag{11}$$

In Eqs. (10)-(11), β is the van't Hoff factor. $\pi_{D,i}$ and $\pi_{F,i}$ are the osmotic pressure of the draw and feed side of the i^{th} membrane segment, $P_{F,i}$ is the hydraulic pressure for segment i. Term $\frac{J_{s,i}}{J_{w,i}}\beta R_g T$ in Eqs. (10) describes alteration of surface osmotic pressure due to the solute diffusion through the membrane. $\left(exp\left(\frac{J_{w,i}}{k_{F,i}}\right) - 1\right)$ denotes the concentration of feed solution while $\left(1 - exp\left(-\frac{J_{w,i}}{K_i}\right)\right)$ represent the dilution of draw solution due to the convection. $k_{F,i}$ is the mass transfer coefficient on the feed-side. K_i is the overall mass transfer coefficient on the draw-side and is obtained by adding the reciprocal of draw-side external mass transfer coefficient, $k_{D,i}$, with that of the internal mass transfer coefficient within the membrane support layer, k_m.

$$\frac{1}{K_i} = \frac{1}{k_m} + \frac{1}{k_{D,i}} \tag{12}$$

k_m can be expressed as a function of the membrane structural parameter S_{OA} and the solute diffusivity coefficient D. In this study, sodium chloride is assumed as the only solute.

$$\frac{1}{k_m} = \frac{D}{S_{OA}} \tag{13}$$

Mass transfer coefficients $k_{D,i}$ and $k_{F,i}$ are calculated by Sherwood correlation shown in Appendix B. The mathematical model is described in greater detail in Appendix B and is validated in Appendix C.

The SEC of the practical OARO system, SEC_{prac}, is derived via substitution of stream properties into Eq. (14) .

$$SEC_{prac} = \frac{P_a \times Q_2 - \eta_{PX}\left(Q_4 \times (P_{RO,B} - P_{OA}) + P_{RO,B} \times Q_5 + P_{OA,B} \times Q_6\right)}{Q_8 \times \eta_{pump}} \tag{14}$$

η_{pump} and η_{PX} are the pump and PX efficiency, respectively. P_a and P_{OA} represent the applied pressure for the RO module and OARO module, respectively, while their corresponding concentrate hydraulic pressures are denoted by $P_{RO,B}$ and $P_{OA,B}$.

2.2.2. The time-of-use (TOU) scenarios

For membrane-based desalination systems, a primary contributor to the UWC is the process energy consumption and hence, the UWC is highly affected by electricity pricing. Apart from the standard flat rate (SFR) electricity pricing (i.e., the electricity price remains constant throughout the day) variable electricity pricing is also considered in this study. Variable electricity pricing is generally represented by the time-of-use (TOU) pricing model. TOU models can promote better matching of electricity demand and production; especially for the highly variable renewable electricity market [37]. The static TOU model adopts an on-and-off-peak pricing structure with predetermined rates. Unlike the static TOU model, the real-time pricing (RTP) structure reflects the dynamic cost margin of electricity. However, it requires hourly-based advance metering infrastructure to store and process customers' consumption profiles [37]. Studies on RTP indicate that customers are reluctant to switch from time-invariant electricity cost structures to RTP, as they fear the potential increase in their electricity bill [23, 37].

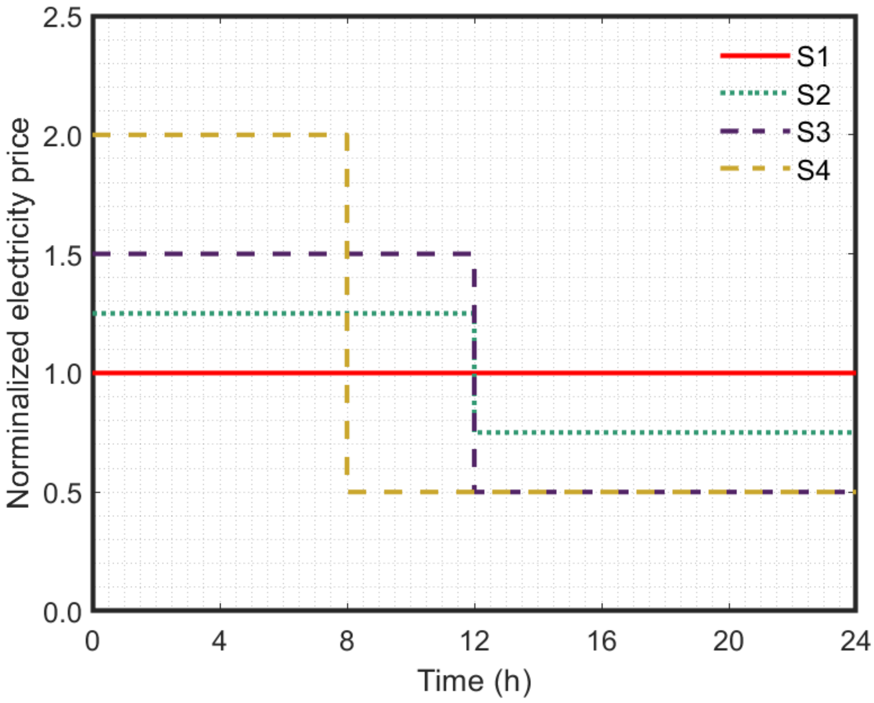

Figure 2. Daily electricity price variations induced by different electricity price regulations. S1: baseline SFR. S2: 25% variance TOU. S3: 50% variance TOU. S4: 50% variance TOU with unequal peak and valley durations.

In this study, the TOU model is employed for the optimization of the CRO and SF-OARO systems in regions with time-varying electricity prices. More specifically, the day-and-night price differentiation static TOU model is employed in this study, owing to its popularity, technical feasibility, and most importantly, a moderate reflection of the time-varying value of electricity. In the SFR scenario, OARO's operating parameters are fixed throughout the day, while in TOU, the operating parameters vary between two pricing periods. As shown in **Error! Reference source not found.**, baseline scenario 1 (S1) describes the conventional SFR electricity price regulation. Apart from the SFR mode, 3 different TOU scenarios (S2-S4) are considered in this study. TOU scenarios have equivalent time-averaged mean values but different durations and peak values. In Scenario 2 (S2), a 25% electricity cost variation from the baseline is assumed with each period lasting 12 hours per day. Peak-hour electricity generation is associated with high carbon emissions and hence, a 50% electricity tariff is adopted as Scenario 3 (S3) to adhere to carbon prices set in stringent environmental regulations [38]. Lastly, Scenario 4 (S4) was added to account for TOU models with an uneven duration of on and off-peak periods.

2.2.3. Unit water cost (UWC) calculation

The SF-OARO plant can be mainly controlled by adjusting four operating variables, namely; (1) the applied pressure to the RO module P_a , (2) the OARO split ratio SR, (3) the feed flowrate per RO pressure vessel (Q_{RO}), and (4) the feed flowrate per OARO pressure vessel (Q_{OA}). These four flow variables, in addition to the number of OARO membrane modules per pressure vessel N_{OA}, are optimised in different scenarios to minimise the UWC of the OARO integrated desalination plant. For the SFR scenario, the operating parameters remain constant throughout the day and hence, can be summarized into a 1x5 input vector $\vec{a}$:

$$\vec{a}_{1\times 5} = \begin{bmatrix} P_a \\ Q_{RO} \\ Q_{OA} \\ SR \\ N_{OA} \end{bmatrix} \tag{15}$$

For a two-period TOU pricing scenario, the flow variables are ideally adjusted among the two electricity pricing periods to minimize the overall UWC. In that case, the optimization input vector $\vec{a}$ is expanded to a 1x9 vector:

$$\vec{a}_{1\times 9} = \begin{bmatrix} P_{a1} \\ Q_{RO1} \\ Q_{OA1} \\ SR_1 \\ N_{OA} \\ P_{a2} \\ Q_{RO2} \\ Q_{OA2} \\ SR_2 \end{bmatrix} \tag{16}$$

The optimization range of each variable contained in the input vector $\vec{a}$ is listed in Table 3.

Table 3 . Variables in OARO system modelling for each optimisation.

		Unit	Upper boundary	Lower boundary
P_{a1}	RO and OARO operating pressure in period 1	bar	120	40
SR_1	Split ratio of RO brine into OARO in period 1	-	3	0
Q_{RO1}	Operating volume flowrate of RO module in period 1	m^3/hr	12	6
Q_{OA1}	Operating volume flowrate of OARO module in period 1	m^3/hr	12	6
N_{OA}	Number of modules in series in one OARO pressure vessel	-	7	4
P_{a2}	Applied pressure to RO module in period 2	bar	120	40
SR_2	Split ratio of RO brine into OARO in period 2	-	3	0
Q_{RO2}	Operating volume flowrate of RO module in period 2	m^3/hr	12	6
Q_{OA2}	Operating volume flowrate of OARO module in period 2	m^3/hr	12	6

The UWC of the CRO and SF-OARO system is calculated using:

$$UWC = \frac{TAC}{AWP} \tag{17}$$

where TAC and AWP are the total annual cost of the system ($/year) and the annual water production (m^3/year), respectively. TAC is comprised of the capital and operational expenditures:

$$TAC = f_c \times CapEx + OpEx \tag{18}$$

The annual capital repayment factor f_c is given by:

$$f_c = \frac{r_i \times (1 + r_i)^{PL}}{(1 + r_i)^{PL} - 1} \tag{19}$$

The lifetime PL of both RO and OARO systems are set to 20 years in this study. The amortised CapEx calculation considers the equipment's depreciation by including the interest rate r_i, the value of which is set to 7.5% [39]. f_c is 10% with a 7.5% interest rate and a 20 year plant life [39].

The capital cost CapEx can be subdivided into the initial purchasing cost of the membrane modules $CapEx_{Mem}$, the cost of the high-pressure pumps $CapEx_{HPP}$ and the booster pumps $CapEx_{BP}$, the cost of the pressure exchangers $CapEx_{PX}$, the cost of the pressure vessels $CapEx_{PV}$ and the cost of intake and pretreatment $CapEx_{In}$. Although the operational expenditure may vary between the two TOU periods, the CapEx remains constant as the installed equipment must be able to handle the maximum required flowrates. Hence, the CapEx calculations are based on the maximum power and membrane requirement among the two TOU periods.

$$CapEx = f_I \times (CapEx_{Mem} + CapEx_{HPP} + CapEx_{BP} + CapEx_{PX} + CapEx_{PV} + CapEx_{In}) \tag{20}$$

f_I is the practical investment factor for osmotic processes [40]. Fouling effect is beyond the scope of this study. Therefore, the redundancies of design factors are neglected for both CRO and SF-OARO systems. SF-OARO has one extra booster pump and more complex flow configuration than CRO, which potentially increase the number of valve and piping. However, such an increase may be diminutive compared to the HPP and membrane cost. Moreover, for SF-OARO, the increment of capital due to added complexity has been reflected in its higher membrane unit cost to CRO. The OpEx is given by electricity O_{Elec}, brine disposal O_B, membrane replacement O_{Re} and maintenance cost O_{Ml}:

$$OpEx = O_{Elec} + O_B + O_{Re} + O_{Ml} \tag{21}$$

In terms of the brine disposal cost, O_B can vary between 0.05-0.3 $/$m^3$ if the brine is directly discharged into surface waters [41]. On the other hand, if the brine is treated prior to disposal to mitigate its environmental impact and comply with desalination brine regulations [42], O_B increases to 0.3-2.64 $/$m^3$ [1, 22]. In this simulation, an intermediate value of O_B (0.3 $/$m^3$) is chosen as benchmark for the cost analysis of the CRO and SF-OARO systems. In Section 3.2.3, the brine cost is also varied to determine its effect on the UWC of the CRO and SF-OARO system. The electricity cost of unit water production is linearly correlated to the total electricity consumption and the electricity price. The calculation is based on the assumption that two different working modes, with different specific energy consumptions (SEC_1 and SEC_2), are used to accommodate for the varying electricity prices between the two TOU periods. SEC_1 and SEC_2 are derived by adding up the energy consumption of the intake and pre-treatment stage (0.3 kWh per m^3 intake) [43], with the osmosis SECs calculated by Eq. (14). The duration of period one t_1 is related to the standard peak-hour electricity price Ep_1 and the second TOU period ($t_2 = 24 - t_1$) is associated with the off-peak hour electricity price Ep_2. Therefore, the total electricity cost per year is calculated by:

$$O_{Elec} = \frac{t_1 \times SEC_1 \times Ep_1 + t_2 \times SEC_2 \times Ep_2}{t_1 + t_2} \times AWP \tag{22}$$

The cost factors used in Eqs. (18)-(22) that are assumed fixed are summarised in Table 4.

Table 4. Cost factors used for the UWC optimisation of the CRO and SF-OARO system [22].

Symbols		Value	Unit	Ref.
$CapEx_{Mem}$	CapEx for membrane	30 (SW30)	\$/m^2	[22]
		50 (AQP)	\$/m^2	[22, 25]
		100 (HPRO)[a]	\$/m^2	[17]
$CapEx_{HPP}$	CapEx for high pressure pump	53	\$/(bar. m^3)	[25]
$CapEx_{BP}$	CapEx for booster pump	53	\$/(bar. m^3)	[25]
$CapEx_{PX}$	CapEx for pressure exchanger	$3134.7 \times {Q_{PX}}^{0.58}$	\$/$(m^3/hr)^{0.58}$	[25]
$CapEx_{PV}$	CapEx for pressure vessel	1000	\$/vessel	[25]
$CapEx_{Intake}$	CapEx for intake and pre-treatment	3170	\$/(m^3/hr intake)	[43]
Ep_{avg}	Average electricity price	0.16	\$/kWh	[44]
f_I	Practical investment factor	1.4	-	[40]
f_c	Annual capital repayment factor	10	%/year	[39]

O_B	Cost of brine disposal	0.3	\$/m^3	[41]
O_{Re}	Cost of membrane replacement	$0.15 \times CapEx_{Mem}$	\$/year	[25]
O_{Ml}	Cost of maintenance and labour	$0.02\ CapEx$	\$/year	[25]

a. HPRO membrane would be applied when the maximum pressure in the module P_a exceeded the maximum operating pressure for SW30 and AQP at 69bar [44].
b. Q_{PX} is the flowrate of stream pass through the pressure exchanger.
c. An extra cost analysis was conducted in Appendix D with identical OARO and RO membrane price.

2.2.4. The optimisation functions

A constrained optimisation function is used to minimise the overall UWC while ensuring that the daily water production target ($Q_{PT} = Q_F \times Y_s$) and the permeate salinity targets in both operating periods (C_{P1}< 0.01 M and C_{P2} < 0.01 M) are met:

$$OPF = f(\vec{a}) = \min\left(W_1 W_2 W_3\left(\left(UWC_1\frac{t_1}{24}\right) + \left(UWC_2\frac{t_2}{24}\right)\right)\right) \tag{23}$$

If the daily water production rate Q_P varies from its target value Q_{PT}, then either the customer's demands are not met, or the excess water cannot be sold. Hence, the penalty factor W_1 is introduced in the optimisation function to prevent this:

$$W_1 = abs\left(\frac{Q_P}{Q_{PT}} - 1\right) \times 20 \tag{24}$$

Similarly, if the target permeate salinity C_{PT} is not met, penalty factors W_1 and W_2 are greater than 1:

$$W_2 = abs\left(\frac{C_{P1}}{C_{PT}} - 1\right) \times 20 \quad if\ C_{P1} > C_{PT} \tag{25}$$

and:

$$W_3 = abs\left(\frac{C_{P2}}{C_{PT}} - 1\right) \times 20 \quad if\ C_{P2} > C_{PT} \tag{26}$$

Utilising MATLAB's built-in fmincon function, with the constraints listed in Table 3, the OPF function can be minimized to obtain the minimal UWC for the given SFR or TOU scenario.

2.3 Optimisation algorithm

The non-linear MATLAB solvers fmincon are firstly used to solve the OPF due to its optimization stability . Three algorithms are underlying fmincon; Levenberg-Marquardt (LM), Trust-Region-Reflective (TRR), and Sequential Quadratic Programming (SQP) [45, 46]. The SQP method requires several analytical derivatives, which are computationally expensive to obtain for this multi-variable optimisation problem. On the other hand, the LM and TRR algorithms are less laborious but still approximate numerically the gradient descent direction [46]. LM, TRR and SQP all rely on the approximation of a gradient, and hence suffer from local convergence [47]. Therefore, it was observed that the optimised UWC is dependent on the initial guess when using fmincon solely.

Hence, a new optimization strategy was used in this study to prevent local convergence. During the optimization process of OPF, a new approach is chosen in which the bio-inspired Porcellio Scaber Algorithm (PSA) method is first used. In the PSA algorithm, the variables are updated using semi-random evolution equations instead of the gradient descent method [48]. A detailed description of the PSA algorithm is offered by Zhang et al. [26] and was also used by Keshta et al. [49] in energy-related optimization problems. Once the PSA algorithm has determined the variables that offer a rough optimum UWC, the OPF was further optimised using the PSA estimated values and fmincon. Using this optimization procedure, a better and stable optimized UWC was obtained for the SF-OARO desalination system at the set target recovery, as shown in Appendix E. Optimization is repeated three times with different initial guesses to ensure the consistency of the optimized result.

3. Results and discussion

3.1 Ideal case study

The results of the optimized ideal specific energy consumption, SEC_{ideal} at different system recoveries

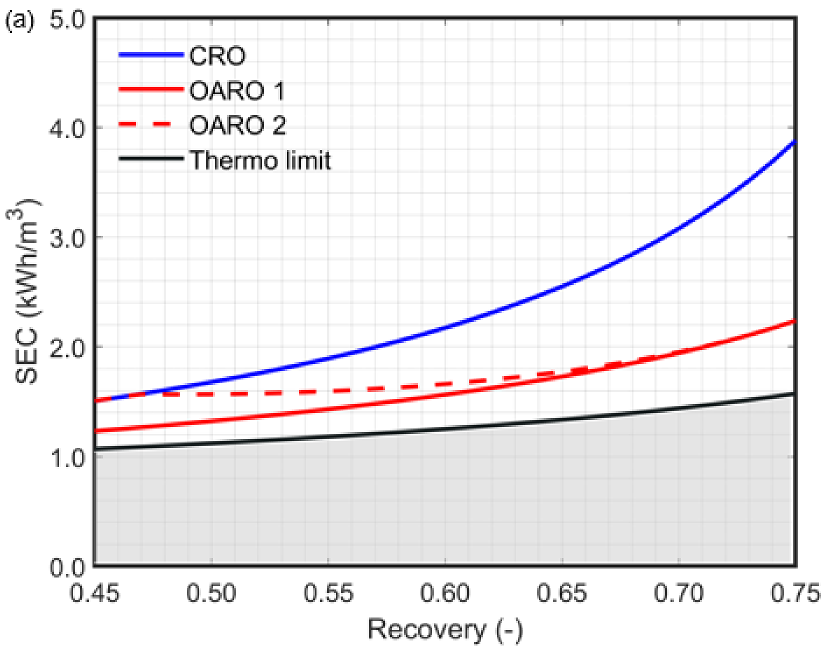

are plotted in

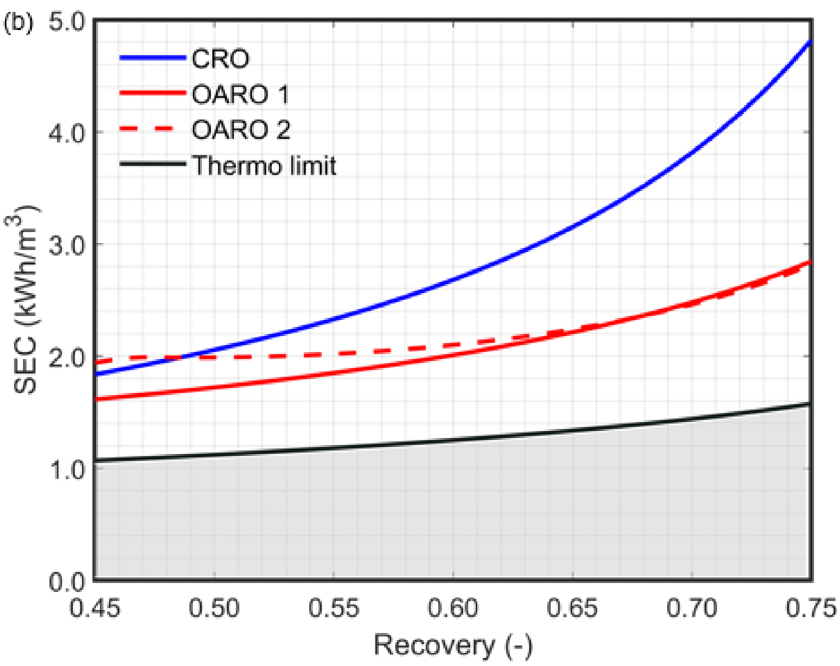

Figure *3*(a). The theoretical SEC of the SF-OARO designs was lower than that of the CRO system. The use of the split feed OARO system with a counter-current design effectively narrowed the osmotic pressure difference across the OARO membrane. Design 1 (OARO 1) can ideally concentrate a 0.6 M seawater feed to 1.5 M at a SEC of 1.56 kWh/m^3. On the other hand, in design 2 (OARO 2), the OARO stage is operated at the same pressure as the RO stage, and hence slightly deviates from its optimal operating pressure. In this case, the energy loss due to over pressurisation in the OARO stage cannot be recovered, which led to a higher SEC than for OARO 1 for the ideal case scenario. With an increase in process recovery, the gap between the optimal pressure of the OARO and the RO stages narrowed. Therefore, the SEC discrepancy between two designs gradually reduces from 7% at RR_S =

0.5 to 0.4% at RR_S = 0.75. At a lower recovery range (45% - 55%), both designs 1 and 2 had an insignificant SEC advantage over CRO. Although working at a much lower pressure than CRO, the mixing of the seawater feed and the diluted recirculated brine from the SF-OARO process increased the total volume of feed to be pressurised in the SWRO modules, which dampened its SEC advantage over CRO. At high recoveries, the OARO stage ensures a significant reduction in operating pressure and hence, both SF-OARO designs performed at a significantly lower SEC in comparison to CRO. As

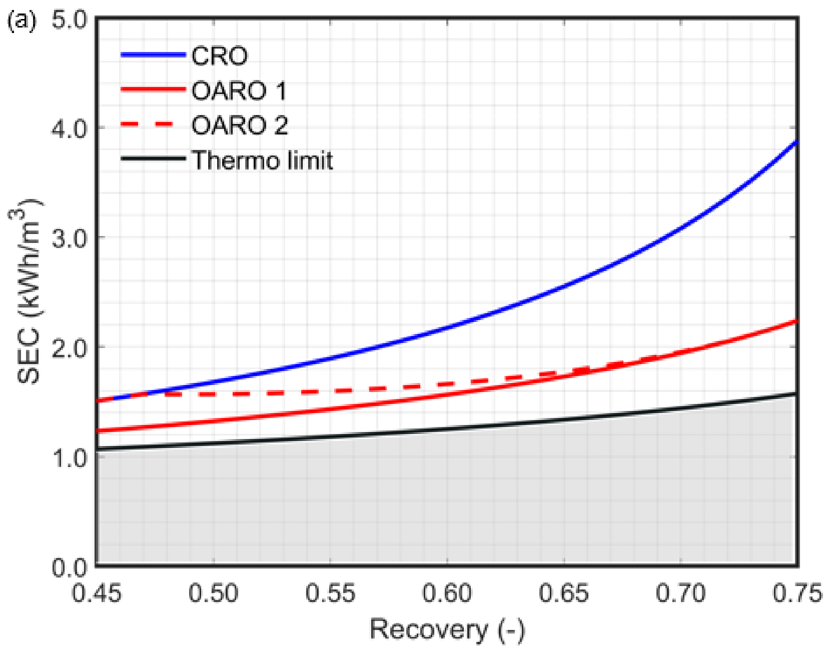

shown in

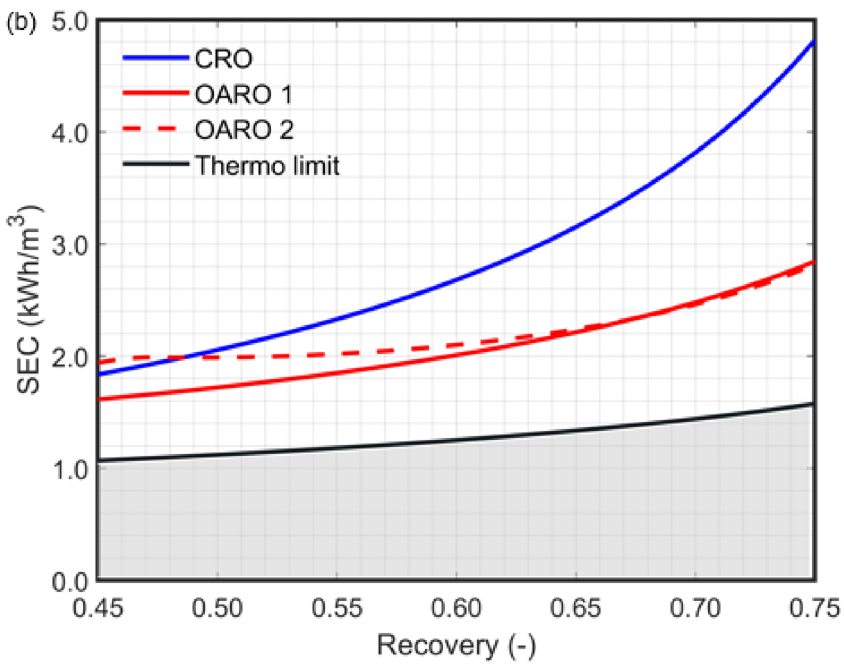

Figure *3* (b), considering pump and PX efficiencies, the more complex design 2 has even higher energy consumption because the added high pressure pump to stream 4 induces additional energy loss during pressurization when compared to design 1.Therefore, design 1 is chosen as it requires less equipment, which will inevitably lower the UWC of the process. Hence, only the SF-OARO design 1 is modelled in the subsequent sections.

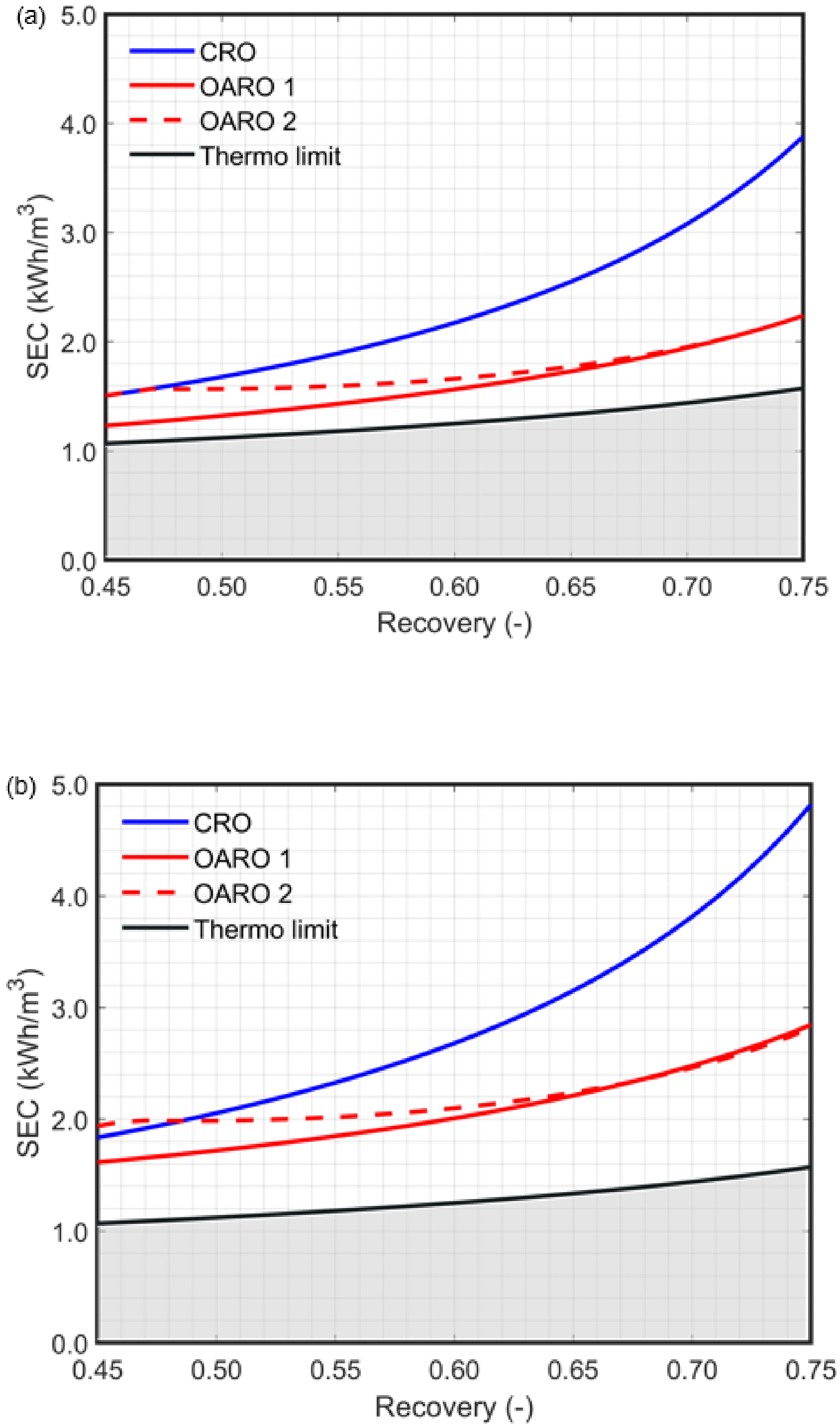

Figure 3. The SEC for the two SF-OARO designs and the CRO system (a) neglecting pump and PX defficiencies, and (b) assuming 80% pump efficiency and 98% PX efficiency. Both scenarios assume no pressure loss and negligible CP effects.

3.2 Practical case Standard flat rate (SFR) scenario.

In this subsection, the focus is on the cost analysis of the SF-OARO (Design 1) and CRO system while assuming the SFR electricity scenario. This means that all operating parameters remained constant throughout the day. Additional assumptions include a constant intake capacity of $20000\ m^3/h$ and a maximum target permeate salinity C_{PT} of 0.01 M. It is important to note that concentration polarization, pump and PX efficiencies, pressure losses and finite membrane areas are considered in this and subsequent sections. The active membrane area of each OARO and RO membrane module is assumed to be equivalent to that of the Dupont SW30-8040 module (37.2 m^2 per module).

3.2.1. Influence of the membrane structural parameter on the specific energy consumption

Figure 4 depicts the applied pressure (Figure 4 (a)) and the SEC (Figure 4 (b)) for both the SF-OARO and the CRO systems. Within the selected recovery domain, the practical SF-OARO design lowered the required operating pressure, which is consistent with the ideal case study. A commercial AQP FO membrane, manufactured by A/S in Copenhagen, was chosen as the benchmark OARO membrane due to its adequate mechanical strength and moderate S-value of 0.6 mm [28]. As shown in Figure 5(a), The SF-OARO system can achieve a 45%, 50%, 65% and 75% recovery at P_a of 47, 52 ,69 and 92 bar, respectively. On the other hand, the maximum operating pressure for the CRO system increases from 60 bar to 150 bar over the same recovery range. Hence, the overall pressure reduction is more significant at higher recoveries and ranges from 15 bar (RR_S = 45%) to 57 bar (RR_S = 75%). The lower operating pressure of the SF-OARO system can have economic benefits, especially when 52% < RR_S < 65%, as the SF-OARO process can be operated at pressures below the membrane manufacturers suggested maximum operating pressure of the SW30 membrane (69 bar). Hence, the use of more expensive HPRO membrane modules can be avoided altogether in the SF-OARO process, which is not possible when operating the CRO process at the same recoveries. Additionally, a reduction in operating pressure contributes to energy savings. For example, as shown in Figure 4 (b), when RR_S = 50% and 65%, the SEC of the SF-OARO system (S_{OA} = 0.6mm) is 2.35 kWh/m^3 and 3.00 kWh/m^3 respectively, which is 7% and 18% lower than that of the CRO system operated at the same recovery level. At the maximum evaluated recovery of RR_S = 75%, the SEC of the SF-OARO process is 3.48kWh/m^3, which is 35% less than that of the CRO process. Both the SEC and P_a results indicate that the SF-OARO system is more suitable for high-recovery operations. However, at lower recoveries

(RR_S < 48%) the SF-OARO process consumes more energy than its CRO counterpart. This can be attributed to the inefficiencies of the OARO stage (e.g., caused by ICP) and due to brine recirculation and the volume increase in saline water to be treated by the RO stage to produce the same amount of permeate.

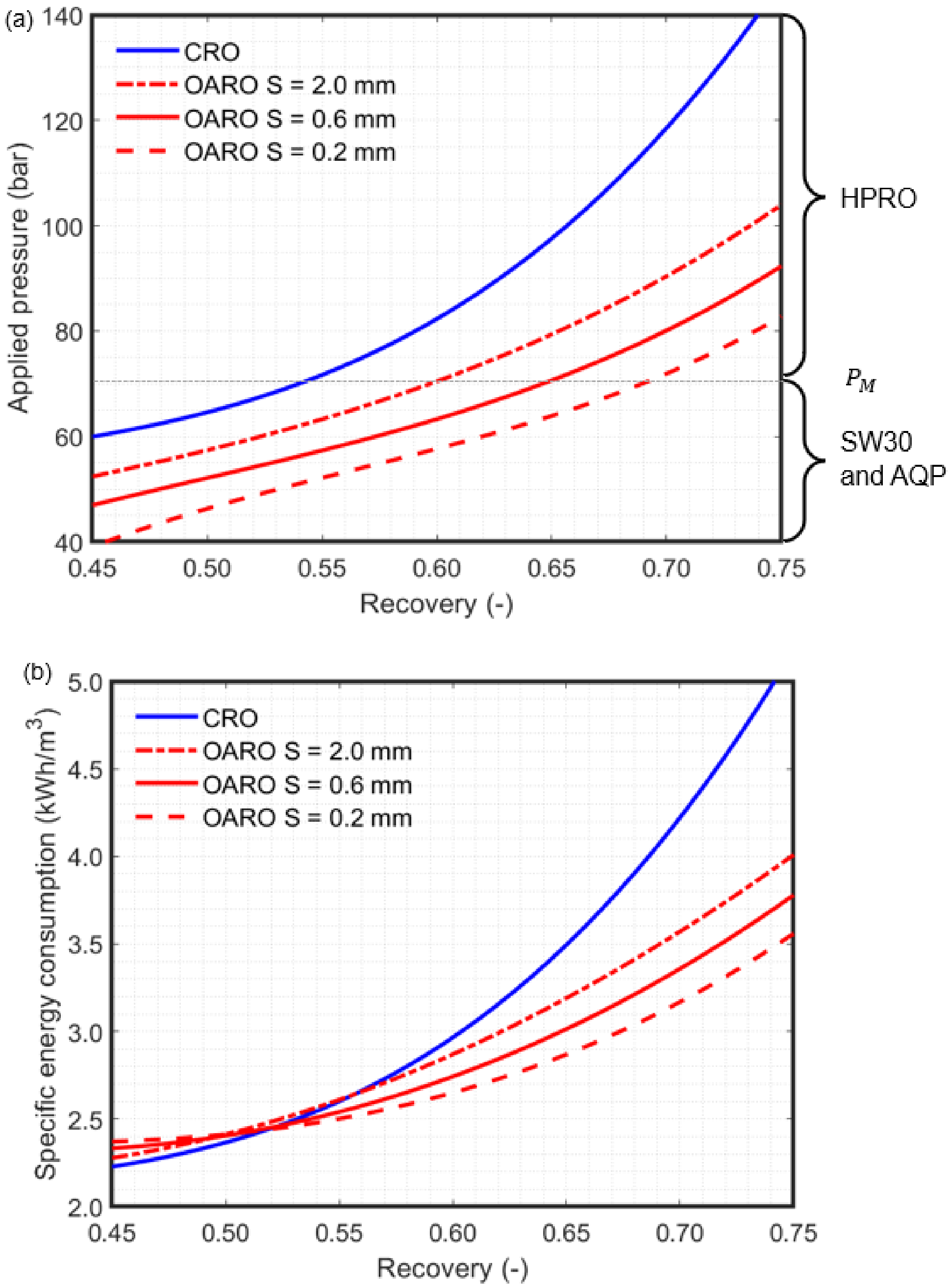

Figure 4. a) Pressure applied to SF-OARO system and b) Specific energy consumption using membranes with different structural parameters of 0.2 mm (dotted red) [50], 0.6 mm (solid red) [31] and 2.0 mm (red dash) [51] in the OARO module. P_M is the membrane pressure threshold above which HPRO membranes are applied.

ICP is the major resistance to the OARO water flux. In the chosen AL-FS design, the ICP effect lowers the effective concentration of the draw solution within the membrane's support layer, which inevitably increases the effective osmotic pressure difference across the active layer. The required operating pressure and the SEC therefore increase with a more significant ICP effect. ICP is dependent on the membrane's structural parameter S and hence, utilising state-of-the-art osmotic membranes with a lower *S* value can effectively reduce the SEC of the OARO system [52].

To examine the effect of ICP on the SF-OARO process performance, 3 different *S*-values were investigated to account for the application of typical RO membranes (S = 2.0 mm) [51], commercial FO membranes (S = 0.6 mm) [31] and a thinner and more porous novel FO membrane (S = 0.2 mm) [50]. Membranes designed for RO have a substantially greater overall thickness and S-value compared to FO membranes. Therefore, their maximum operating pressure is greater due to more severe ICP, which led to an increase in the SEC and the operating pressure of the SF-OARO process. The utilisation of novel FO membranes reduced the SEC of the SF-OARO system from 3.00 kWh/m^3 to 2.70 kWh/m^3 at a recovery of 65% However, membranes with a more porous, less tortuous and thinner support layer may suffer from insufficient mechanical strength for high pressure brine dewatering [28]. The AQP (solid red line) membrane was chosen for the SF-OARO cost optimization in the following sections, as it was successfully tested in our previous experimental studies at pressures of up to 60 bar without showing any signs of membrane failure [28].

3.2.2. Total cost breakdown of the CRO+SF-OARO system in SFR scenario

Figure 5 (a) compares the UWC of the SF-OARO and CRO system at different recoveries. The optimal recovery (at which the UWC is at its lowest) of the CRO and SF-OARO process is 50% and 65%, respectively. When operating at the optimal recoveries, the SF-OARO UWC is approximately 4.1% lower than that of the CRO process. This means that CRO desalination plants employing membranes with low maximum operating pressures (69 bar) would benefit from the addition of a OARO stage even if the electricity price remains constant throughout the day. A cost saving of 4.1 % is significant in the desalination market especially for larger desalination plants, such as the Ras Al-Khair plant in Saudi Arabia, which can produce up to 1 million cubic meters of permeate per day [53]. This means that a 4.1% UWC saving can result in annual savings exceeding millions of USD.

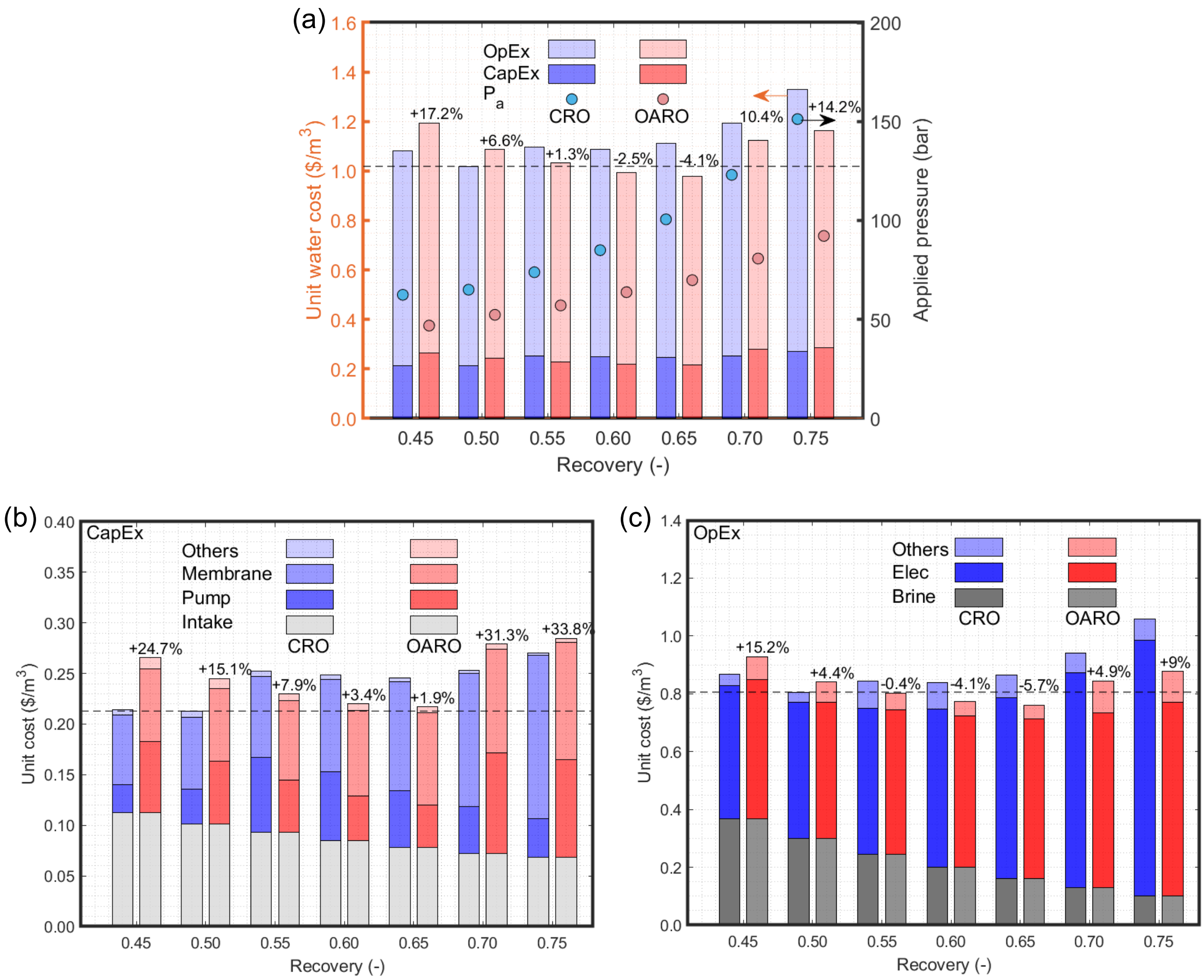

Figure 5. The breakdown of a) UWC b) CapEx and c) OpEx for the SFR electricity scenario of the CRO system (blue) and SF-OARO system (red). The recommended maximum operating pressure for the SW30 and AQP membrane is assumed to be 69 bar. All designs have a fixed constant intake flowrate with the same pre-treatment method and cost.

The breakdown of CapEx for both systems are shown in Figure 5 (b). As previously mentioned, the SF-OARO system can increase the system recovery to 65% without the use of HPRO membrane modules due to the lower required operating pressure. Therefore, compared to the CRO scenario at its optimal recovery of 50%, the optimal SF-OARO system shows an insignificant increase in membrane capital cost. When improving the recovery from 50% to 65%, the high-pressure pump costs for the SF-OARO configuration are 14.5% less than that of the CRO system due to lower operating pressure. As the improved recovery lowers the intake cost per unit of water production, only a 1.9% increase in CapEx is observed for the SF-OARO system (RR_S =65%) compared to the 50%-recovery CRO.

Table 5. Average water flux and membrane area for optimized SF-OARO and CRO system with 20,000 m^3/hr intake capacity at 50%, 65% and 75% recovery.

Process	Recovery	RO module average $J_{w,i}$	OARO module average $J_{w,i}$	SW30 (m^2)	AQP (m^2)	HPRO (m^2)	$\frac{CapEx_{HPP}}{AWP}$ (\$/m^3)	$\frac{CapEx_{BP}}{AWP}$ (\$/m^3)	$\frac{CapEx_{PX}}{AWP}$ (\$/m^3)
CRO	50%	13.7	-	7.30×10^5	-	-	0.07	0.002	0.003
	65%	24.9	-	-	-	5.21×10^5	0.11	0.002	0.003
	75%	37.8	-	-	-	3.94×10^5	0.16	0.001	0.002
SF-OARO	50%	9.6	13.7	1.04×10^6	1.65×10^5	-	0.07	0.004	0.004
	65%	15.5	14.5	8.44×10^5	1.93×10^5	-	0.09	0.003	0.003
	75%	14.5	14.8	-	-	1.24×10^6	0.12	0..003	0.002

The average water flux in each membrane module of the CRO and SF-OARO system is presented in Table 5. At 65% recovery, the CRO system is operated at higher applied pressure than SF-OARO. Due to the significant osmotic pressure difference between the front and rear solution in the CRO process, over-pressurization of the feed solution at the front element is severe. The SF-OARO system has an added OARO stage compared to the CRO. Therefore, the front-and-rear osmotic pressure differences inside the membrane modules of the SF-OARO system are less significant than those inside the membrane modules of the CRO system. The feed solution at the front element of membrane modules in the SF-OARO system is less over pressurized. The average water flux of high-recovery CRO processes are significantly higher than SF-OARO and currently operating CRO (at 50% recovery). Therefore, in practical high-recovery CRO, the capital and operational costs are potentially higher than the simulated result due to extra fouling prevention effort or increased membrane area to reduce water flux. If the CRO at 65% and 75% recoveries have similar water flux as CRO at 50% recovery, the membrane area will increase to 9.49×10^5 and 1.10×10^6 m^2, respectively. Therefore, if operated at a similar average water flux, the total membrane area of SF-OARO at 65% and 75% recovery are less than 10% higher than the CRO at the same recoveries. The Capex for high pressure pump contributes to the majority of the capital cost for pumping system. As recovery increases, the capital cost of the high pressure pump increases with recovery for both CRO and SF-OARO while the capital cost for booster pump and pressure exchanger decreases. Cost for PX and BP only account for less than 10% of the Capex for the pumping system.

On the other hand, the OpEx of the SF-OARO process is less than that of the CRO system when the recovery exceeds 53% due to the lower SEC and reduced membrane maintenance cost. Figure 5 (c) shows how the two main OpEx contributors (i.e., electricity and brine disposal cost) vary with the process recovery. As expected, the energy demand and hence electricity cost of both the CRO and SF-OARO systems increase with the system recovery while the brine disposal cost decreases. However, as shown in Figure 5 (c), the increase in the osmosis-related electricity cost is less significant with the recovery for the SF-OARO system. Combined with a significant reduction of brine disposal volume, the operational cost of the 65% recovery SF-OARO system is 5.7% less than the 50% recovery CRO.

Uncertainties remain as to whether the OARO membrane modules can be operated at pressures up to 69 bar. The AQP membrane modelled in this study was previously tested and found stable at pressures up to 60 bar when using an RO permeate carrier and a 3D printed spacer backing [28]. The stability of the AQP membrane may be affected at such high operating pressures and under long-term operation, which would mean that the actual maximum operating pressure may be less than 69 bar. In addition, the active membrane area of the AQP membrane module may be lower than commercial SWRO module which may increase the amount of pressure vessel applied to SF-OARO. Additional uncertainties are focused on membrane fouling. Generally speaking, fouling is more severe at higher recoveries due to the concentration of foulants within the feedwater (SF-OARO is operated at 65% whereas CRO operated at 50%). Hence, more rigorous pre-treatment might be required for the SF-OARO process. It is interesting to note that in a previous study on the comparison of fouling in forward osmosis (FO) and RO, it was found that the more severe fouling in FO would not lead to more significant flux decline due to the strong internal concentration polarization (ICP) self compensation effect in FO [54]. Therefore, it can be speculated that even though the fouling might be more severe at higher recoveries in SF-OARO, flux decline in OARO process might not be more significant than that at lower recoveries due to the ICP self-compensation effect in OARO. Therefore, in our calculation, we assume the same pretreatment strategy is sufficient to prevent significant flux decline due to fouling even at the highest recovery. A more systematic study is required to correlate flux decline, fouling/scaling and water recovery ratio in the OARO process in the future. Nonetheless, the presented UWC results at constant electricity pricing (SFR scenario) highlight the potential benefits of the SF-OARO system and should be attainable with further membrane development, as was carried out by Liang et al [55].

3.2.3. Influence of the brine disposal cost and electricity price on the UWC

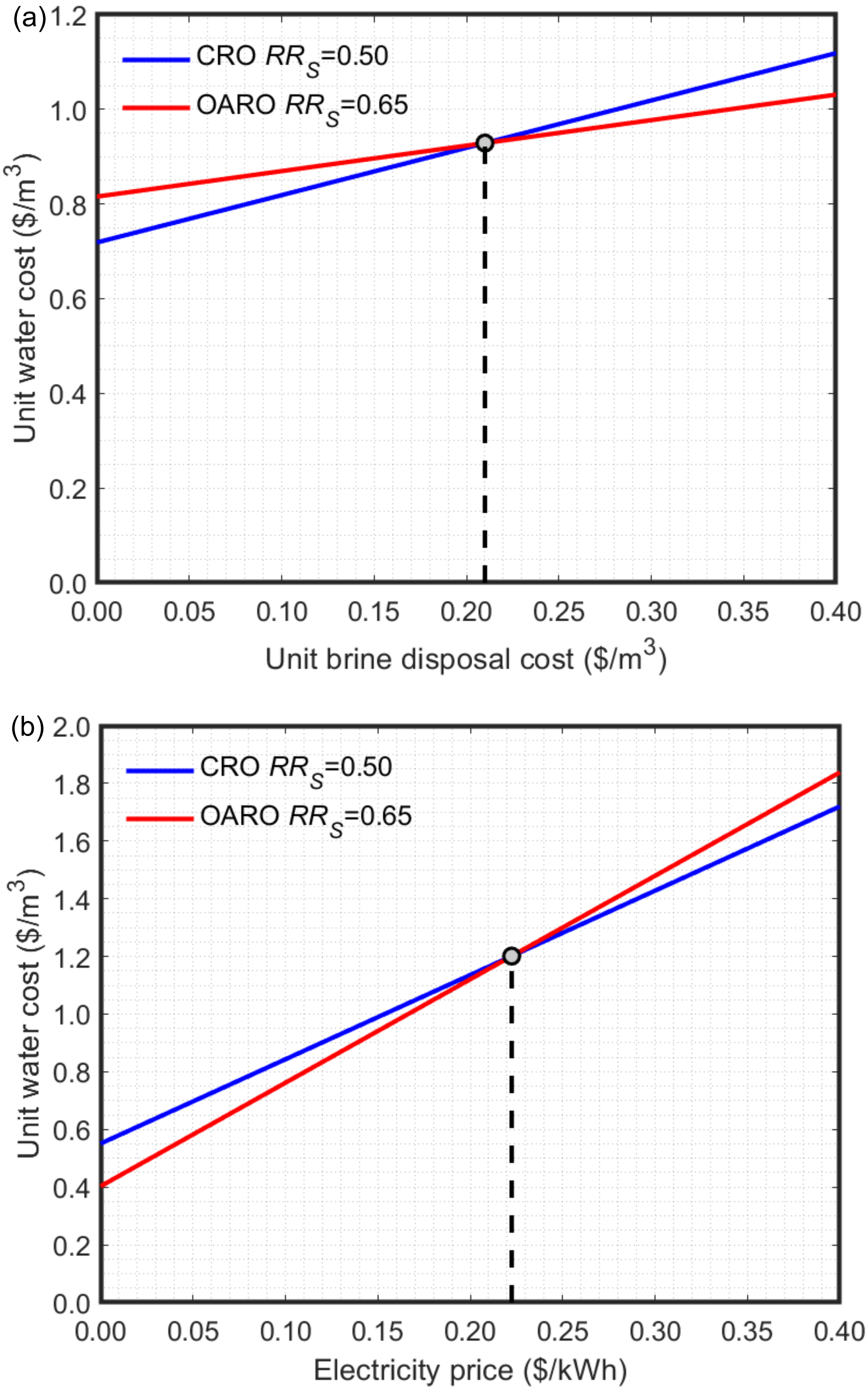

Figure 6. UWC of the CRO system at RR_s = 0.50 (blue) compared with the OARO system for RR_s=0.65 (red) at (a) brine disposal price from 0-0.4 $/m^3 and (b) electricity price from 0-0.4 $/kWh. The operating parameter is assumed to be identical to the optimized values in Section 3.2.2.

The impact of brine disposal cost and electricity price on the UWC is further investigated in Figure 6. In general, the SF-OARO process is preferred in regions with higher brine disposal costs and when the electricity price is lower. For the given operating conditions and system constraints, the SF-OARO process is the preferred choice, once the brine disposal cost exceeds 0.21 $\$/m^3$, as its lower brine volume is disposed of at lower cost. Although the environmental impact of brine is widely disputed [7, 8], several environmental regulations are in place that further increase the cost of coastal and in-land brine disposal [7], which makes the use of high-recovery membrane processes, such as the presented SF-OARO system, more attractive. In addition to the typical surface discharge of brine, other brine disposal methods are also more expensive, such as sewer discharge, deep-well injection, discharge into evaporation ponds, and land applications [6]. The 4.1% of UWC saving shown in Figure 5 (a) is based on the current electricity price of Singapore, 0.16 $/ kWh. As the SEC of the SF-OARO process (RR_S = 65%) is higher than that of the CRO process at a 50% recovery, the cost savings offered by the SF-OARO process would increase if the electricity cost could be lowered further, while the CRO process remains the more economic choice when electricity pricing is higher than 0.22 $/kWh, assuming identical optimal operating parameter as in Section 3.2.2. The SEC of the SF-OARO process can, however, further be lowered when utilising membranes with a lower S-value (i.e., reduction in ICP).

3.3 Practical case: Time-of-use (TOU) scenarios

In this subsection, the UWC is estimated for both the SF-OARO and CRO systems for the three different TOU scenarios. The overall recovery for the SF-OARO and CRO system are fixed at 65% and 50%, according to the optimal result in shown in Figure 5. Although the electricity price varies between peak and valley hours, the overall, daily average electricity rate remains constant and equivalent to that of the SFR mode.Table 6 shows how the maximum operating pressure and the SEC change with the TOU scenarios during the different peak and valley electricity rate periods. Period 1 is where the electricity prices are higher, while in period 2 the electricity prices are lower. As shown by the optimized results, the operating pressure is higher in period 2 for all three TOU scenarios (Scenario 2-4) to lower the overall UWC, as more water is produced when the electricity is cheaper. Hence, the UWC of the SF-OARO and CRO system take advantage of the low electricity prices in the low-demand period via a variable plant operating strategy. It is assumed that the feed flowrate is fixed and hence, if the water production increases in one period then it reduces in the other so that the overall daily water production rate remains constant. Hence, the water production was curtailed during peak-electricity pricing to save energy costs. However, this operating strategy requires extra capacity to produce sufficient amounts of water in the low-electricity pricing period. Therefore, the overall CapEx was increased to cover the additional production volume in period 2 while operating at lower recoveries in period 1 (when electricity is more expensive) and resulted in a lower water flux and less efficient use of the membrane stages.

Table 6. Optimized applied pressure and SEC of 2-period variate-mode operation of the CRO system at 50% recovery and the SF-OARO system at RR_S=65% under 4 different electricity tariff scenarios. Scenario 1 is the SFR scenario.

Scenario	System and recovery	P_{a1} period 1 (bar)	P_{a2} period 2 (bar)	SEC period 1 (kWh/m^3)	SEC period 2 (kWh/m^3)
1	CRO, RR_S = 50%	66.0	66.0	2.36	2.36
	SF-OARO, RR_S = 65%	69.9	69.9	2.99	2.99
2	CRO, RR_S = 50%	65.8	66.2	2.36	2.36
	SF-OARO, RR_S = 65%	68.8	70.3	2.95	3.00
3	CRO, RR_S = 50%	65.8	66.2	2.36	2.36
	SF-OARO, RR_S = 65%	68.5	69.9	2.94	2.98
4	CRO, RR_S = 50%	63.9	66.6	2.30	2.38
	SF-OARO, RR_S = 65%	69.1	70.1	2.97	3.00

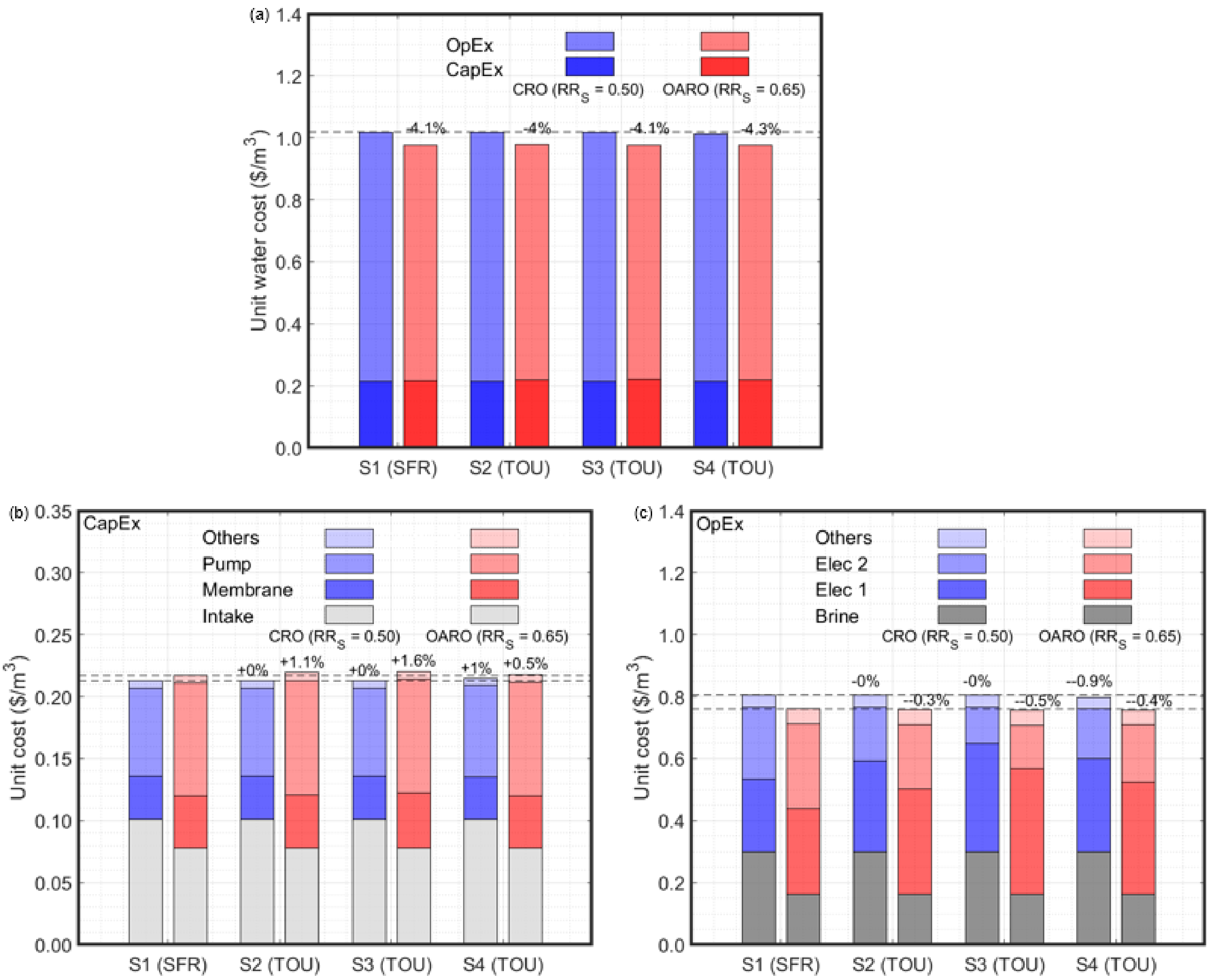

Figure 7. Breakdown of the a) UWC b) CapEx and c) OpEx for the CRO (blue) and SF-OARO system (orange) in optimal conditions for the different scenarios. S1: baseline SFR. S2: 25% variance TOU. S3: 50% variance TOU. S4: 50% variance TOU with unequal peak and valley durations. The total recovery for the CRO and OARO system are set to be 50% and 65% respectively according to the optimal result obtained from Figure 5. Elec 1 and Elec 2 are the contribution of electricity cost to OpEx for period 1 and 2 respectively.

Figure 7 (a) compares the UWC of CRO and SF-OARO, based on the three different TOU models. The attribution of the OpEx and CapEx in different electricity tariff scenarios are shown in Figure 7 (b) and (c). In the first two TOU scenarios (S2 and S3), the duration of peak and valley electricity periods is equal. The electricity prices during peak pricing increased 25% and 50% above the SFR electricity price in S2 and S3, respectively. In S4, the peak pricing period is shorter but 100% more expensive than the SFR electricity price. Changing from SFR to TOU electricity pricing is beneficial for reducing the UWC of the SF-OARO system, whereas the UWC of CRO remains unaffected. Dynamic SF-OARO operation can lead to an additional UWC reduction of 0.1%-0.3% (S2-S4). This is due to a lowering of the OpEx, as depicted in Figure 7 (c), which was more significant than the increase in CapEx arising from excess membrane and pump capacity required during the low electricity pricing period, as shown in Figure 7 (b). On the other hand, CRO can only enhance the process recovery by increasing the operating pressure and hence, the reduction of UWC by variate operation is inconspicuous in a different electricity pricing scenario. In SF-OARO, the recovery is not only adjusted by altering the operating pressure but also by changing the split ratio SR. For example, when a higher process recovery is required, the volume of the OARO draw solution is increased leading to a higher brine recirculation in the SF-OARO system. This added flexibility offered by SF-OARO leads to the additional UWC savings and hence, makes it an ideal process for dynamic operation, especially when the pricing in the two operating periods varies significantly as in S4.

4. Conclusion

The presented results highlight that the SF-OARO process can be more cost-efficient than the conventional, single-stage RO process under the given operating conditions when stringent brine disposal regulations are implemented. This study utilizes 0.3 $/m^3 brine disposal charge and 0.16 $ /kWh average electricity price as benchmark conditions. At constant electricity pricing, the SF-OARO process can be operated at a 4.1% lower UWC while achieving a higher process recovery (RR_S = 65% in comparison to CRO ($RR_S = $ 50%). The benefit of adding an OARO stage to the process is especially evident when the RO membrane burst pressure is low (69 bar) and when the brine cost is high. The SF-OARO process would greatly benefit from an OARO membrane that can withstand high operating pressures while having a low S-value to minimize ICP. Reducing ICP will further reduce the SEC and the capital cost of the SF-OARO process.

For the different TOU electricity scenarios, the CRO UWC remains constant as the recovery can only be adjusted via pressure alterations. On the other hand, the SF-OARO UWC can be lowered during dynamic operation. The ratio between OARO feed and draw volume can be adjusted during dynamic operation, which gives the SF-OARO system the necessary flexibility to operate under ideal conditions for any of the given TOU scenarios. Although the SF-OARO process is more complex than the CRO process, the added flexibility on operation and the savings in UWC are beneficial, especially when large scale plants can save 3-4% of their UWC.

Acknowledgements

This research was supported by the Ministry of Education, Singapore, under the Academic Research Fund Tier 1 (RG84/19).

Appendix A. Derivation of SEC for the ideal case study

For both designs, the pressure applied in the RO module equals the maximum osmotic pressure difference within the unit. Hence, for both designs 1 and 2, $P_{RO} = \pi_3 = \beta R_g T C_3$. As friction loss is neglected, 2 modules have the same operating pressure in design 1, $P_{RO} = P_{OA}$. Substituting stream properties from *Table 1,* the ideal SEC for design 1 can be derived as:

$$SEC_{d1,ideal} = \frac{P_a \times Q_2 - P_{OA} \times (Q_6 + Q_5)}{Q_8}$$
$$= \frac{\beta R_g T C_3 \times \left(\frac{1 - RR_S}{1 - RR_{OA}} \times (SR + 1) + RR_S - \frac{1 - RR_S}{1 - RR_{OA}} \times SR - (1 - RR_S)\right)}{RR_S} \tag{27}$$
$$= \frac{\beta R_g T C_{sw} \left(\frac{1 - RR_S}{1 - RR_{OA}} + 2RR_S - 1\right)(1 - RR_{OA})}{RR_S(1 - RR_S)}$$

For the second design, two modules operated at different pressures $P_{OA} \neq P_a$. The optimal applied pressure equals P_{OA} the maximum transmembrane osmotic pressure difference within the OARO module,

$$P_{OA} = \pi_6 - \pi_5 = \beta R_g T C_{sw} \times \frac{RR_{OA}}{(1 - RR_S)} \tag{28}$$

Ideally, stream 4, 5 and 6 would be depressurised to ambient pressure. HPP-2 repressurised Stream 4 to the target OARO operating pressure P_{OA}, therefore,

$$SEC_{d2,ideal} = \frac{P_a \times Q_2 + P_{OA} \times Q_4 - (P_a \times Q_3 + P_{OA} \times Q_6)}{Q_8} =$$
$$= \frac{\beta R_g T C_{SW} \left((C_6 - C_5)(1 - RR_S)\left(\frac{1}{1 - RR_{OA}} - 1\right) + \frac{1 - RR_{OA}}{1 - RR_S} RR_S\right)}{RR_S} \tag{29}$$
$$= \frac{\beta R_g T C_{SW} \left(\frac{{RR_{OA}}^2}{1 - RR_{OA}} + \frac{1 - RR_{OA}}{1 - RR_S} RR_S\right)}{RR_S}$$

For both designs, the optimal SEC_{ideal} was obtained by minimising the 2-variable function $SEC_{ideal} = f(RR_{OA}, SR)$ using the MATLAB fmincon function. The practical SEC was estimated with the pumping and pressure exchange deficiency of $\eta_{pump} = 80\%$ and $\eta_{PX} = 98\%$ respectively. For design 1, the SEC with deficiency was calculated as:

$$SEC_{d1,deff} = \frac{P_a \times Q_2 - \eta_{PX}\left(P_a \times (Q_6 + Q_5)\right)}{Q_8 \times \eta_{pump}}$$
$$= \frac{\beta R_g T C_{SW}(1 - RR_{OA}) \times \left(\left(\frac{(1 - RR_S)(SR + 1)}{1 - RR_{OA}} + RR_S\right) - \eta_{PX} \times \left(\frac{(1 - RR_S) \times SR}{1 - RR_{OA}} + (1 - RR_S)\right)\right)}{(1 - RR_S)RR_S \times \eta_{pump}} \quad (30)$$

For the second design considering pump and PX deficiencies:

$$SEC_{d2,deff} = \frac{P_a \times Q_2 + P_{OA} \times Q_4 - \eta_{PX}(P_a \times Q_3 + P_{OA} \times Q_6)}{Q_8 \times \eta_{pump}}$$
$$= \beta R_g T C_{SW} \frac{\frac{(1 - RR_{OA})}{1 - RR_S} \times \left(\frac{1 - RR_S}{1 - RR_{OA}} \times (SR + 1) + RR_S\right) + \frac{RR_{OA}}{1 - RR_{OA}} - \eta_{PX}\left((SR + 1) + RR_{OA}\right)}{RR_S \times \eta_{pump}} \quad (31)$$

Appendix B. FDM model of RO and OARO module

The stream properties of the SF-OARO system is calculated via combining a trail-and-shoot mass-balance calculation procedure with the FDM computational framework for RO and OARO membrane processes developed by Bartholomew [35]. The mass transfer coefficient on feed and draw side of the membrane channel, $k_{F,i}$ and $k_{D,i}$ is calculated by Sherwood correlation[56],

$$k_{F\ or\ D,i} = Sh\frac{D}{d_h} \quad (32)$$

$$Sh = 0.28Re^{0.57}\ Sc^{0.40} \quad (33)$$

d_h is the hydraulic diameter of the membrane channel, Sh, Re and Sc are the Sherwood, Reynolds number and Schmidt number of the solution in the membrane channel corresponding to the mass transfer coefficient, respectively.

The input of each set of SF-OARO mass balance calculation is the constant stream 1 properties Q_1=20000 m^3/hr, C_1=C_{sw}=0.6 M and the operating parameters P_a , Q_{RO}, Q_{OA}, RR and N_{OA}. The number of trails is defined as j. At the first shoot, $j = 1$, an initial guess of the properties of stream 7, $Q_{7,j=1}$, $C_{7,j=1}$ is applied to derive properties of stream 2, Q_2 and C_2. The number of RO pressure vessels, $n_{PV,RO}$, can be derived by,

$$n_{PV,RO} = \frac{Q_2}{Q_{RO}} \tag{34}$$

Q_{RO}, $C_{2,}$, serve as the input to the RO FDM model to obtain the stream properties of the RO outflow, Q_3, C_3 and $P_{RO,B}$. Q_4 and Q_5 is calculated by Eq.(4) while $C_5 = C_4 = C_3$, $P_{OA} = P_{RO,B}$. The number of OARO modules are derived by,

$$n_{PV,OA} = \frac{Q_5}{Q_{OA}} \tag{35}$$

P_{OA}, Q_4, Q_5 and $n_{PV,OA}$ are applied in the OARO FDM model to derive its outflows properties including Q_6, $Q_{7,new}$, C_6, $C_{7,new}$ $and P_{OA,B}$, Q_7 and C_7 obtained from the j^{th} shooting are applied to derive the Q_2 and C_2 of the $(j+1)^{th}$ shooting. The trial and shoot iterations are repeated until the difference between the $Q_{7,new}$ and $C_{7,new}$from the $(j+1)^{th}$ shooting and those from the j^{th} shooting is less than 0.01%. The derivation of stream properties is summarized in *Figure B-1*.

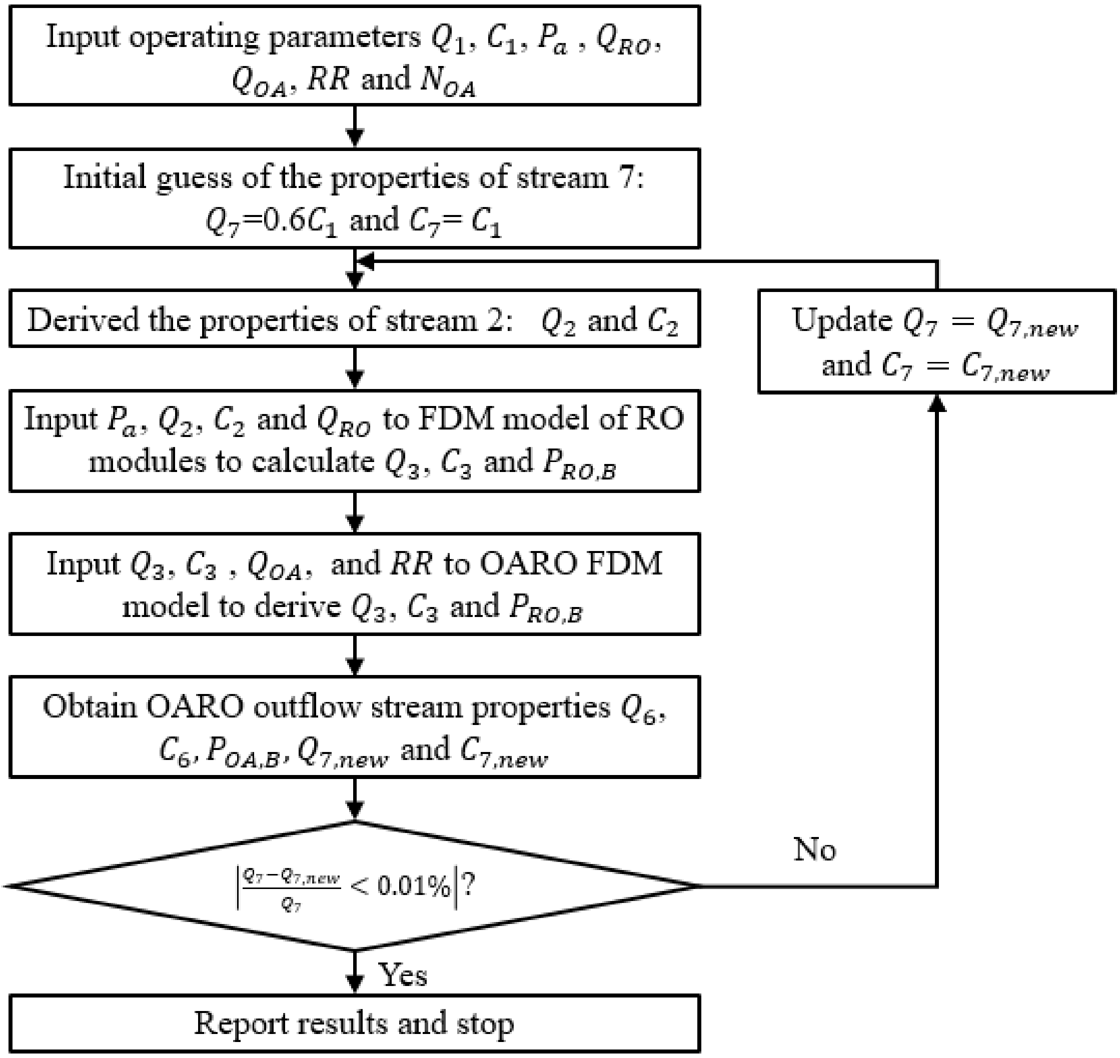

Figure B-1. The algorithm to derive stream properties for SF-OARO system.

Appendix C. Validation of RO and OARO simulation

The FDM model of CRO was validated by WAVE (The Water Application Value Engine), a water processing analysis software developed by Dupont. The error margin of applied pressure derived from the FDM model is less than 0.2%. As shown in Figure C-1, the difference between the FDM model and WAVE result is less than 0.7%.

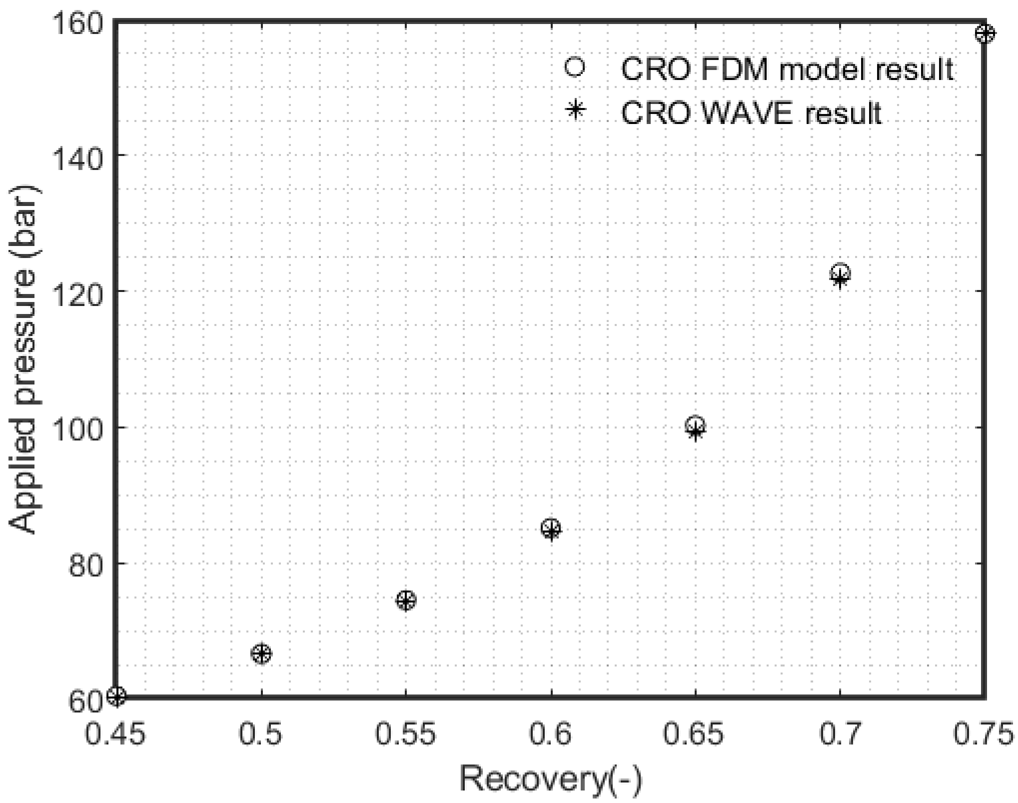

Figure C-1. Applied pressure at different recovery obtained from CRO model compared with WAVE. Both results are obtained from 7-module RO pressure vessel with the membrane area of 37.2 m^2.

Appendix D. UWC calculated by equivalent membrane price

The UWC result in Section 3.2.2 is sensitive to the price of membranes chosen in each scenario. Although the recommended operating pressure for CRO is 69 bar considering the long-term stability of the system[15], which is also the operating pressure for many of the current RO desalination plants [57], the novel commercial Dupont SW30 membrane can operate at the maximum pressure of 82 bar. However, the extreme scenario of 82 bar would induce severe membrane compaction and have a negative effect on the cost of high-pressure pumping and piping. Nevertheless, as technologies advance, additional costs for high-pressure operation might be diminished. Moreover, as large-scale fabrication of AQP and HPRO membranes become mature in the future, their price is expected to drop. We still conduct 2 extra cost analyses using 1) high-pressure threshold and 2) equal price for all types of membrane respectively, to exam the suitability of the OARO project in the new generation of desalination.

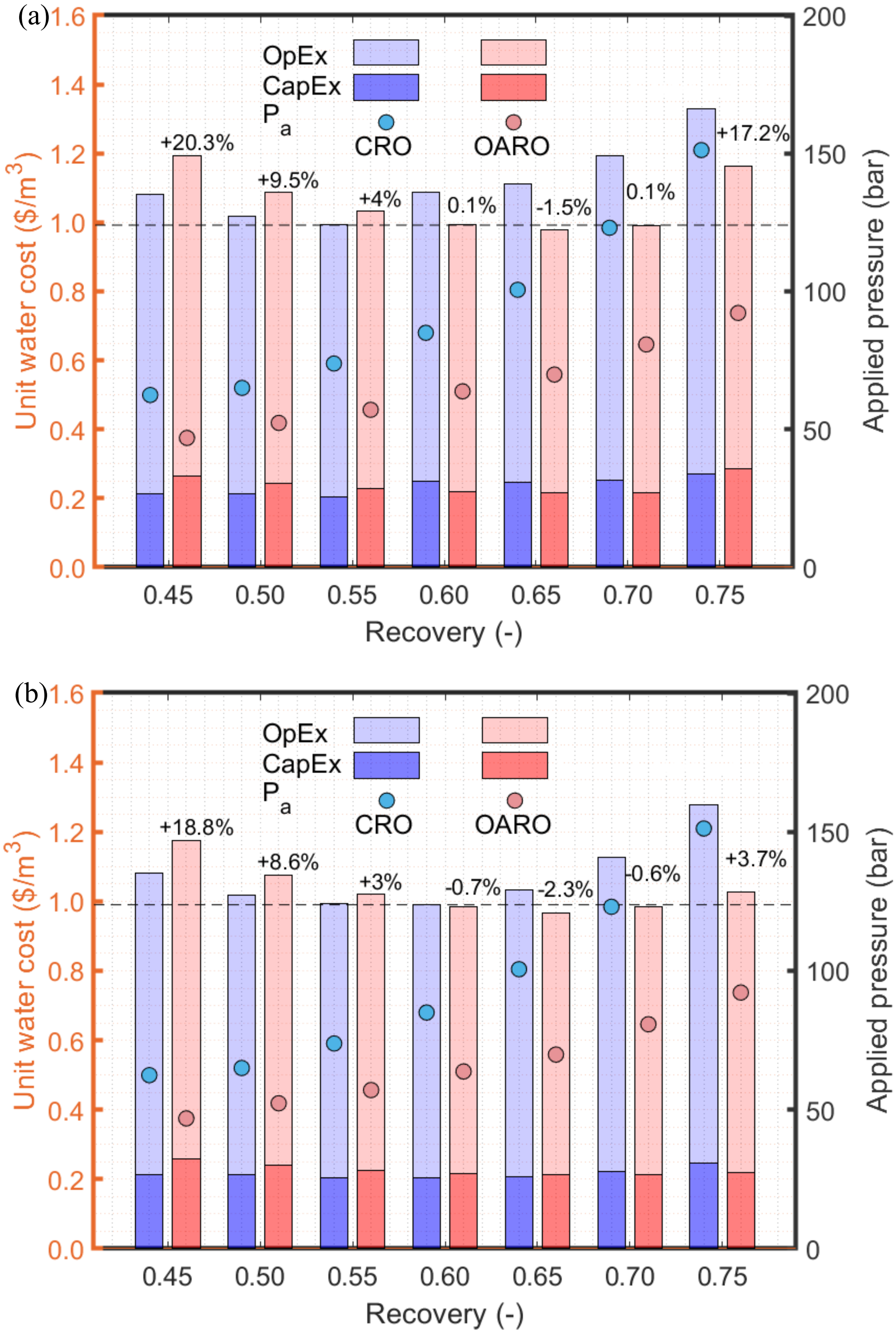

Figure D-1. CapEx and OpEx components of estimated UWC for SPF mode two-stage OARO system (blue) and one-stage RO system (red) assuming a) membrane burst pressure at 82 bar, b) HPRO, OARO and RO membrane at the constant unit area price of 30 \$/m^2.

The result from *Figure D-1* shows that the optimal recovery of the OARO process remains constant in both scenarios. The UWC value altered insignificantly compared to the result in Section 3.2.2.

However, the optimal UWC of CRO is further reduced when the pressure threshold is increased for the SWRO membrane, but the UWC of the optimal OARO is still 1.5% less than its competitor, CRO. If the constant unit price is assumed for all types of membranes, the OARO system can have a 2.3% reduction of UWC over the CRO.

Appendix E. Comparison between the result from PSA and gradient method

Table E-1. Optimal average applied pressure obtained by the different algorithms in variate electricity tariff S1 scenarios for Y_s= 65%.

Method	Initial guess of period 1 pressure (bar)	Optimised pressure	Iteration number
GD	50	51.1	
	60	59.6	300
	70	68.8	
	80	73.5	
PSA+GD	10 randomized initial guesses between 40-100	68.8	500

Table E-1 shows that the conventional gradient descent (GD) generated various results from different initial guesses because the model of variate mode OARO system comprised multiple that caused multiple local minima. Moreover, the evolution of variables in GD was based on the gradient of the existing point. Therefore, the optimal value calculated by stand-alone GD was highly dependent on its initial guess. Furthermore, the implicitness of the OARO model and its inconspicuous gradient resulted in inefficient gradient descent. By integration with PSA, the GD method gave more consistent results than stand-alone GD. Unlike stand-alone GD, the GD algorithm in the PSA+GD method was fed with an initial guess generated by the PSA, which was closed to the global optimal point. The PSA algorithm circumvented the local convergence and inefficiency of the GD by its semi-discrete evolutions of variables. To explain further, the update between variable generations in PSA were partially randomized and partially toward the best-value point. The gradient-based calculation was not involved in PSA, which improved its efficiency in solving the implicit and highly non-linear OARO model. Moreover, the PSA method had multiple randomized initial guesses to balance their effect on convergence, avoiding the result leaning to a single guess value. The efficiency of the PSA method can be further enhanced by alternating the randomization factor (RF) to achieve optimal balance between the convergence rate and accuracy. If RF=0, the update of variables was fully randomized, ignoring the current optimal values [26]. Ideally, the whole domain of variables was searched to derive a guaranteed global optimal condition; however, the iteration time became unacceptable. When RF=1, the variables converged toward the current optimal point within a few iterations. The result had a high dependency on the initial guess due to insufficient iteration. With a moderate RF value=0.6, the 9-variable optimal function converged to a rough global minimum within only 500 iterations. Adding 300 additional iterations of GD calculation, PSA+GD converged stably to a consistent global optimal point. The accuracy of optimal results in this study was supported by the fact that the optimal flowrate applied pressure and *SR* split ratio derived are consistent with the previous OFAT study on the OARO process [20]. Hence, the PSA+GD method effectively optimized the condition for the multi-variate non-linear OARO desalination process with a moderate computational load.

References

[1] T.M. Missimer, R.G. Maliva, Environmental issues in seawater reverse osmosis desalination: Intakes and outfalls, Desalination, 434 (2018) 198-215.
[2] S. Miller, H. Shemer, R. Semiat, Energy and environmental issues in desalination, Desalination, 366 (2015) 2-8.
[3] J.R. Werber, A. Deshmukh, M. Elimelech, Can batch or semi-batch processes save energy in reverse-osmosis desalination?, Desalination, 402 (2017) 109-122.
[4] M. Elimelech, W.A. Phillip, The future of seawater desalination: Energy, technology, and the environment, Science, 333 (2011) 712-717.
[5] D.E.a.W. Authority, DEWA Selects Preferred Bidder For 120 MIGD Hassyan Sea Water Reverse Osmosis (SWRO) IWP Project, in, Wateronline, 2021.
[6] J. Morillo, J. Usero, D. Rosado, H. El Bakouri, A. Riaza, F.-J. Bernaola, Comparative study of brine management technologies for desalination plants, Desalination, 336 (2014) 32-49.
[7] N. Ahmad, R.E. Baddour, A review of sources, effects, disposal methods, and regulations of brine into marine environments, Ocean & Coastal Management, 87 (2014) 1-7.
[8] O. Ogunbiyi, J. Saththasivam, D. Al-Masri, Y. Manawi, J. Lawler, X. Zhang, Z. Liu, Sustainable brine management from the perspectives of water, energy and mineral recovery: A comprehensive review, Desalination, 513 (2021).
[9] B. Al-Najar, C.D. Peters, H. Albuflasa, N.P. Hankins, Pressure and osmotically driven membrane processes: A review of the benefits and production of nano-enhanced membranes for desalination, Desalination, 479 (2020).
[10] E. Cardona, A. Piacentino, F. Marchese, Energy saving in two-stage reverse osmosis systems coupled with ultrafiltration processes, Desalination, 184 (2005) 125-137.
[11] J. Swaminathan, E.W. Tow, R.L. Stover, J.H. Lienhard, Practical aspects of batch RO design for energy-efficient seawater desalination, Desalination, 470 (2019).
[12] D.M. Warsinger, E.W. Tow, K.G. Nayar, L.A. Maswadeh, V.J. Lienhard, Energy efficiency of batch and semi-batch (CCRO) reverse osmosis desalination, Water Res, 106 (2016) 272-282.
[13] K. Park, P.A. Davies, A compact hybrid batch/semi-batch reverse osmosis (HBSRO) system for high-recovery, low-energy desalination, Desalination, 504 (2021).
[14] D.M. Davenport, A. Deshmukh, J.R. Werber, M. Elimelech, High-Pressure Reverse Osmosis for Energy-Efficient Hypersaline Brine Desalination: Current Status, Design Considerations, and Research Needs, Environmental Science & Technology Letters, 5 (2018) 467-475.
[15] D.M. Davenport, C.L. Ritt, R. Verbeke, M. Dickmann, W. Egger, I.F.J. Vankelecom, M. Elimelech, Thin film composite membrane compaction in high-pressure reverse osmosis, Journal of Membrane Science, 610 (2020).
[16] J. Spence, A.S. Tooth, Pressure vessel design: concepts and principles, CRC Press, 2012.
[17] C. Dickerson, M. Mirabolghasemi, A Comparative Produced Water Management Decision Making WorkFlow: MSEEL Case Study, in: SPE Western Regional Meeting, OnePetro, 2021.
[18] Z. Wang, A. Deshmukh, Y. Du, M. Elimelech, Minimal and zero liquid discharge with reverse osmosis using low-salt-rejection membranes, Water Res, 170 (2020) 115317.
[19] A.T. Bouma, J.H. Lienhard, Split-feed counterflow reverse osmosis for brine concentration, Desalination, 445 (2018) 280-291.
[20] C.D. Peters, N.P. Hankins, Osmotically assisted reverse osmosis (OARO): Five approaches to dewatering saline brines using pressure-driven membrane processes, Desalination, 458 (2019) 1-13.

[21] X. Chen, N.Y. Yip, Unlocking High-Salinity Desalination with Cascading Osmotically Mediated Reverse Osmosis: Energy and Operating Pressure Analysis, Environ Sci Technol, 52 (2018) 2242-2250.
[22] C.D. Peters, N.P. Hankins, The synergy between osmotically assisted reverse osmosis (OARO) and the use of thermo-responsive draw solutions for energy efficient, zero-liquid discharge desalination, Desalination, 493 (2020).
[23] Y. Wang, L. Li, Time-of-use electricity pricing for industrial customers: A survey of U.S. utilities, Applied Energy, 149 (2015) 89-103.
[24] F. Edition, Guidelines for drinking-water quality, WHO chronicle, 38 (2011) 104-108.
[25] T.V. Bartholomew, N.S. Siefert, M.S. Mauter, Cost Optimization of Osmotically Assisted Reverse Osmosis, Environ Sci Technol, 52 (2018) 11813-11821.
[26] Y. Zhang, S. Li, H. Guo, Porcellio scaber algorithm (PSA) for solving constrained optimization problems, arXiv preprint arXiv:1710.04036, (2017).
[27] S. Kayaci, S.B. Tantekin-Ersolmaz, M.G. Ahunbay, W.B. Krantz, Technical and economic feasibility of the concurrent desalination and boron removal (CDBR) process, Desalination, 486 (2020).
[28] C.D. Peters, D.Y.F. Ng, N.P. Hankins, Q. She, A novel method for the accurate characterization of transport and structural parameters of deformable membranes utilized in pressure- and osmotically driven membrane processes, Journal of Membrane Science, 638 (2021).
[29] D.W. Solutions, FILMTEC™ Membranes. Product Information Catalog, in, 2017.
[30] dupont, SW30HRLE-400, (2020).
[31] A.P. Straub, N.Y. Yip, M. Elimelech, Raising the bar: Increased hydraulic pressure allows unprecedented high power densities in pressure-retarded osmosis, Environmental Science & Technology Letters, 1 (2014) 55-59.
[32] M. Askari, C.Z. Liang, L.T. Choong, T.-S. Chung, Optimization of TFC-PES hollow fiber membranes for reverse osmosis (RO) and osmotically assisted reverse osmosis (OARO) applications, Journal of Membrane Science, 625 (2021).
[33] I.B. Cameron, R.B. Clemente, SWRO with ERI's PX Pressure Exchanger device — a global survey, Desalination, 221 (2008) 136-142.
[34] Dupont, SW30-4040 dupont, (2019).
[35] T.V. Bartholomew, M.S. Mauter, Computational framework for modeling membrane processes without process and solution property simplifications, J. Membr. Sci., 573 (2019) 682-693.
[36] Q. She, R. Wang, A.G. Fane, C.Y. Tang, Membrane fouling in osmotically driven membrane processes: A review, J. Membr. Sci., 499 (2016) 201-233.
[37] M. Harding, S. Sexton, Household Response to Time-Varying Electricity Prices, Annual Review of Resource Economics, 9 (2017) 337-359.
[38] R. Hledik, W. Gorman, N. Irwin, M. Fell, M. Nicolson, G. Huebner, The value of TOU tariffs in Great Britain: Insights for decision-makers, Citizen Advice, Final Report, 1 (2017).
[39] P. Pazouki, R.A. Stewart, E. Bertone, F. Helfer, N. Ghaffour, Life cycle cost of dilution desalination in off-grid locations: A study of water reuse integrated with seawater desalination technology, Desalination, 491 (2020).
[40] M.N.A.H. A. Malek, J.C. Ho, Design and economics of RO seawater desalination, Desalination, 105 (1996) 245-261.
[41] J.R. Ziolkowska, R. Reyes, Prospects for Desalination in the United States—Experiences From California, Florida, and Texas, in: Competition for Water Resources, 2017, pp. 298-316.
[42] S. Liyanaarachchi, L. Shu, S. Muthukumaran, V. Jegatheesan, K. Baskaran, Problems in seawater industrial desalination processes and potential sustainable solutions: a review, Reviews in Environmental Science and Bio/Technology, 13 (2013) 203-214.
[43] N. Voutchkov, Energy use for membrane seawater desalination – current status and trends, Desalination, 431 (2018) 2-14.

[44] S. Government, Electricity Tariffs, in, 2021.
[45] MathWorks, fmincon, in: Solver-Based Nonlinear Optimization, 2020.
[46] K. Levenberg, A method for the solution of certain non-linear problems in least squares, Quarterly of applied mathematics, 2 (1944) 164-168.
[47] L. Bottou, Stochastic gradient descent tricks, in: Neural networks: Tricks of the trade, Springer, 2012, pp. 421-436.
[48] Y. Zhang, P. Zhang, S. Li, PSA: A novel optimization algorithm based on survival rules of porcellio scaber, in: 2021 IEEE 5th Advanced Information Technology, Electronic and Automation Control Conference (IAEAC), IEEE, 2021, pp. 439-442.
[49] H.E. Keshta, O.P. Malik, E.M. Saied, F.M. Bendary, A.A. Ali, Energy management system for two islanded interconnected micro-grids using advanced evolutionary algorithms, Electric Power Systems Research, 192 (2021).
[50] X. Li, C.H. Loh, R. Wang, W. Widjajanti, J. Torres, Fabrication of a robust high-performance FO membrane by optimizing substrate structure and incorporating aquaporin into selective layer, Journal of Membrane Science, 525 (2017) 257-268.
[51] B. Kim, G. Gwak, S. Hong, Review on methodology for determining forward osmosis (FO) membrane characteristics: Water permeability (A), solute permeability (B), and structural parameter (S), Desalination, 422 (2017) 5-16.
[52] L. Shen, X. Zhang, L. Tian, Z. Li, C. Ding, M. Yi, C. Han, X. Yu, Y. Wang, Constructing substrate of low structural parameter by salt induction for high-performance TFC-FO membranes, Journal of Membrane Science, 600 (2020).
[53] A. Bennett, Advances in desalination energy recovery, World Pumps, 2015 (2015) 30-34.
[54] F.A. Siddiqui, Q. She, A.G. Fane, R.W. Field, Exploring the differences between forward osmosis and reverse osmosis fouling, J. Membr. Sci., 565 (2018) 241-253.
[55] C.Z. Liang, M. Askari, L.T.S. Choong, T.S. Chung, Ultra-strong polymeric hollow fiber membranes for saline dewatering and desalination, Nat Commun, 12 (2021) 2338.
[56] Q. She, D. Hou, J. Liu, K.H. Tan, C.Y. Tang, Effect of feed spacer induced membrane deformation on the performance of pressure retarded osmosis (PRO): Implications for PRO process operation, Journal of Membrane Science, 445 (2013) 170-182.
[57] J. Kim, K. Park, D.R. Yang, S. Hong, A comprehensive review of energy consumption of seawater reverse osmosis desalination plants, Applied Energy, 254 (2019).